JIMD Reports
DOI 10.1007/8904_2015_427

RESEARCH REPORT

Clinical Severity of PGK1 Deficiency Due To a Novel p.E120K Substitution Is Exacerbated by Co-inheritance of a Subclinical Translocation t(3;14)(q26.33;q12), Disrupting *NUBPL* Gene

Dezső David · Lígia S. Almeida · Maristella Maggi · Carlos Araújo · Stefan Imreh · Giovanna Valentini · György Fekete · Irén Haltrich

Received: 25 November 2014 / Revised: 11 February 2015 / Accepted: 19 February 2015 / Published online: 27 March 2015

Abstract Carriers of cytogenetically similar, apparently balanced familial chromosome translocations not always exhibit the putative translocation-associated disease phenotype. Additional genetic defects, such as genomic imbalance at breakpoint regions or elsewhere in the genome, have been reported as the most plausible explanation.

By means of comprehensive molecular and functional analyses, additional to careful dissection of the t(3;14)(q26.33;q12) breakpoints, we unveil a novel X-linked PGK1 mutation and examine the contribution of these to the extremely severe clinical phenotype characterized by hemolytic anemia and neuromyopathy.

The 3q26.33 breakpoint is 40 kb from the 5′ region of tetratricopeptide repeat domain 14 gene (*TTC14*), whereas the 14q12 breakpoint is within IVS6 of nucleotide-binding protein-like gene (*NUBPL*) that encodes a mitochondrial complex I assembly factor. Disruption of *NUBPL* in translocation carriers leads to a decrease in the corresponding mRNA accompanied by a decrease in protein level. Exclusion of pathogenic genomic imbalance and reassessment of familial clinical history indicate the existence of an additional causal genetic defect. Consequently, by WES a novel mutation, c.358G>A, p.E120K, in the X-linked phosphoglycerate kinase 1 (*PGK1*) was identified that segregates with the phenotype. Specific activity, kinetic properties, and thermal stability of this enzyme variant were severely affected. The novel *PGK1* mutation is the primary genetic alteration underlying the reported phenotype as the translocation per se only results in a subclinical phenotype. Nevertheless, its co-inheritance presumably exacerbates PGK1-deficient phenotype, most likely due to a synergistic interaction of the affected genes both involved in cell energy supply.

Communicated by: Gregory Enns

Competing interests: None declared

Electronic supplementary material: The online version of this chapter (doi:10.1007/8904_2015_427) contains supplementary material, which is available to authorized users.

D. David (✉) · L.S. Almeida · C. Araújo
Department of Human Genetics, National Institute of Health Dr Ricardo Jorge, Lisbon, Portugal
e-mail: dezso.david@insa.min-saude.pt

M. Maggi · G. Valentini
Department of Biology and Biotechnology "L. Spallanzani", University of Pavia, Pavia, Italy

M. Maggi
Department of Molecular Medicine, Unit of Immunology and Pathology, University of Pavia, Pavia, Italy

S. Imreh
Microbiology and Tumour Biology Center, Karolinska Institute, Stockholm, Sweden

G. Fekete · I. Haltrich
II Department of Pediatrics, Semmelweis University, Budapest, Hungary

Introduction

There is an intriguing group of apparently balanced familial chromosomal translocations characterized by phenotypic inconsistency among carriers of cytogenetically similar rearrangements.

The most fascinating explanation for this would be the co-inheritance of the chromosomal translocation with a mutation at the same or at a distinct genetic *locus*, leading to a recessive monogenic or digenic disorder. Such a case

has not yet been described so far (Schäffer 2013). On the contrary, genomic imbalance at breakpoint regions is the most plausible explanation of such phenotypic inconsistency observed among carriers of similar chromosomal translocations (De Gregori et al. 2007).

Presently, the lack of a fully annotated human genome, including a haploinsufficiency map, hinders predictability of the phenotypic consequences of balanced chromosomal translocations even when the breakpoints are identified at nucleotide resolution. Although these may considerably affect the genomic architecture at breakpoint regions, a large majority are expected to be phenotypically imperceptible or subclinical. Nevertheless, otherwise subclinical translocations may modulate clinical phenotypes.

In eukaryotes ATP synthesis relies on glycolysis and oxidative phosphorylation (OXPHOS). Phosphoglycerate kinase 1 (PGK1; ATP: 3-phosphoglycerate 1-phosphotransferase; EC 2.7.2.3) is a multifunctional protein with a key role in ATP generation during glycolysis. PGK1 deficiency (OMIM #300653) is an X-linked recessive condition characterized by variable clinical manifestations involving up to three different tissues, i.e., red blood cells (RBC), skeletal muscle, and neurological tissue. However, patients rarely show all three clinical features (Beutler 2007; Chiarelli et al. 2012). To date, 22 different mutations have been identified in *PGK1*, and 17 of them have been characterized at the protein level (Chiarelli et al. 2012; Fermo et al. 2012; Tamai et al. 2014).

Mitochondrial complex I (CI) or NADH-ubiquinone reductase (EC 1.6.5.3) is part of the electron transport chain that results in ATP synthesis through complex V or ATP synthase of the OXPHOS pathway (Fassone and Rahman 2012). At least 12 assembly factors are required for the proper assembly, stability, or maturation of this CI (Fassone and Rahman 2012). One of these assembly factors is NUBPL, the depletion of which causes CI deficiency (OMIM #252010) (Tucker et al. 2012; Kevelam et al. 2013). Incorporation of Fe/S clusters into CI subunits by NUBPL is indispensable for electron transfer activity of CI (Sheftel et al. 2009).

Here we present detailed molecular and functional analyses demonstrating that the phenotype allegedly associated with the chromosome rearrangement t(3;14)(q26.33;q12) is actually due to a novel PGK1 variant, p.E120K, resulting in severe decrease of enzyme activity and that 14q12 breakpoint disruption of mitochondrial CI assembly factor, NUBPL, presumably exacerbates the neuromuscular symptoms of the enzyme deficiency.

Materials and Methods

Samples, Cytogenetic Analysis, and Lymphoblastoid Cell Lines (LCLs)

The family under study is from Hungary. Blood samples were collected after informed consent; the study was carried out according to the Principles of the Declaration of Helsinki of the World Medical Association.

Cytogenetic analyses and the establishment of LCLs were performed as previously described (David et al. 2009).

DNA extraction, flow sorting of derivative (der) chromosomes, array painting, amplification of the junction fragments, and SNP 6.0 array analysis

Genomic DNA extractions, flow sorting, and amplification of der chromosome-specific DNAs were performed as described earlier (David et al. 2009, 2013). Genomic amplicons of der(3) and der(14) chromosomes were analyzed by array painting using CytoScan HD array (Affymetrix, Santa Clara, CA, USA). The der(3) and der(14) junction fragments were amplified (see Table S1 for conditions) and sequenced by Sanger sequencing.

Genomic DNA from the index subject and his brothers (III:3 and III:6) was analyzed by Genome-Wide Human SNP 6.0 array (Affymetrix). Genotype calling was carried out using Genotyping Console software, and data was visualized using the Chromosome Analysis Suite (ChAS) software (Affymetrix).

Whole-Exome Sequencing (WES)

Exonic targets were captured and enriched using the SureSelect Human All Exon 50 Mb Kit from Agilent Technologies (Santa Clara, CA, USA) and sequenced on a HiSeq2000 instrument (Illumina, San Diego, CA) following the manufacturer's instructions. Variants were annotated, and known SNPs as well as novel genetic alterations were identified.

RNA Extraction and Expression Studies

Extraction of RNA samples from LCLs and reverse transcription (RT) reactions were performed as described earlier (David et al. 2013). For real-time quantitative PCR (RT-qPCR), see supplementary material.

Expression profiling of LCLs from the index subject and III:3 was carried out using the Human Gene 1.0 ST expression array (Affymetrix), and data analysis was performed as previously described (David et al. 2013).

Construction of the Expression Vector Coding for PGK1 p.E120K Variant

The vector encoding PGK1-E120K variant was obtained by subjecting pMM1 to site-directed mutagenesis using Quick Change XL site-directed mutagenesis kit (Stratagene, La Jolla, CA, USA) (Chiarelli et al. 2012). Mutagenic oligonucleotides are available in supplementary material.

Expression, Purification, and Characterization of the PGK1-E120K Variant

The PGK1-E120K was expressed in *E. coli* BL21(DE3) pLysS cells grown on ZYP-5052 autoinducing medium. The expressed enzyme variant was purified essentially as previously described (Chiarelli et al. 2012). Enzymatic activity and kinetic and thermal stability analyses have been performed (see the supplementary material).

SDS-PAGE and Immunodetection

SDS-PAGE analysis was performed in control and subjects' LCL's pellets (15 μg protein). For immunodetection the following antibodies were used: rabbit anti-NUBPL (Mitosciences, Eugene, OR, USA), mouse anti-tubulin (Sigma, St. Louis, USA), and MitoProfile Total OXPHOS antibody cocktail (Mitosciences, Eugene, OR, USA). Quantification was performed using the Quantity One (BioRad) software.

Results

Clinical Report

The first reported symptom of the index subject (Fig. 1, III:5) was neonatal hyperbilirubinemia. Transfusion therapy was necessary at the age of eight months because of severe anemia, jaundice, and hepatomegaly, leading to the diagnosis of idiopathic hemolytic anemia. His dysmorphic features resembled those of his affected brother III:4 (Supplementary Material and Table S2), but, additionally, brachycephaly, short neck, reduced length of phalanges, four-digit crease on the right palm, cutaneous syndactyly II/III of the feet, and severe hypotonia were also reported (Fig. S2C). Repeated therapy-resistant seizures started at one year of age, and his unconscious stage resulted in a suspected but unconfirmed diagnosis of meningoencephalitis. Besides epilepsy, one of the hemolytic events caused stroke and hemiparesis of the left side. Cognitive and somatic development of the child stopped at the age of one year and 6 months: he did not walk and could not speak, but he had no hearing loss. Swallowing difficulties became more and more pronounced; gastrostoma and tube feeding were initiated from the age of 2 years. Severe recurrent hemolytic crises led to a partial splenectomy at the age of four and a half years. Positron emission tomography revealed Rasmussen's encephalitis at 5 years of age. At 6 years of age, ketogenic diet was initiated.

At the age of thirteen years, in 2013, he presented total body muscle atrophy, generalized somatic hypotrophy, diminished joint movements, muscle contractures, severe somato-mental retardation, no speech and no personal contact with other individuals, multiple dental caries, and bilateral cryptorchidism. The eyes are "swimming."

Two of his brothers (Fig. 1, III:3 and III:6) are healthy. In general, psychomotor development of III:3 was normal. He did not present any dysmorphic features. Reportedly, with physical effort, he shows signs of weakness and premature fatigue, well before his age-matched coworkers (Table 1).

Both parents are healthy, but the mother (II:5), in addition to anemia during pregnancies, also presents signs of fatigue.

During the course of this study, a maternal male cousin (Fig. 1, III:2), who died after falling down the stairs at the age of 7 years, was reported to have symptoms similar to his cousins.

His mother (II:3) and the remaining relatives (I:2, II:1, III:1) are all healthy. For additional clinical description, including subjects III:4 and III:2, see supplementary material.

Cytogenetic Analysis

Cytogenetic analysis of GTL-banded metaphase chromosomes performed on subject III:4 revealed an apparently balanced reciprocal chromosome translocation between the long arms of chromosomes 3 and 14 [46,XY,t(3;14)(q26.3;q12)] (Fig. S2A and B). Furthermore, his healthy mother (II:5) and two of his brothers (III:3 and III:5) were also carriers of a similar translocation (Fig. 1a).

No perfect co-segregation between the translocation and the reported phenotype could be observed; therefore, we hypothesized that an additional genomic or genetic defect might also segregate in this family.

Breakpoints and Candidate Genes

Genomic amplicons of flow-sorted der chromosomes were analyzed by array painting, and the breakpoints were narrowed to few kb regions (data not shown). Primers flanking the predicted breakpoints were designed, and the junction fragments were amplified and sequenced (Table S1). The alterations revealed by sequence alignments of the junction fragments are summarized in Fig. S1.

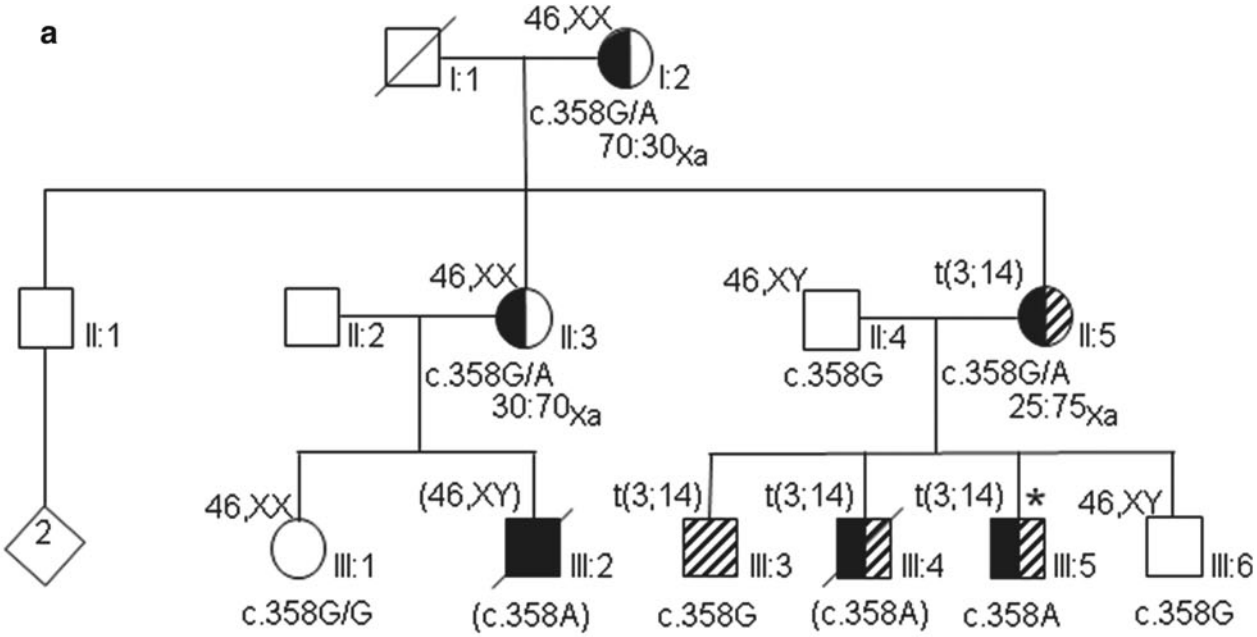
a
46,XX
I:1
I:2
c.358G/A
70:30Xa
II:1
II:2
46,XX
II:3
c.358G/A
30:70Xa
46,XY
II:4
c.358G
t(3;14)
II:5
c.358G/A
25:75Xa
2
46,XX
III:1
c.358G/G
(46,XY)
III:2
(c.358A)
t(3;14)
III:3
c.358G
t(3;14)
III:4
(c.358A)
t(3;14)
*
III:5
c.358A
46,XY
III:6
c.358G

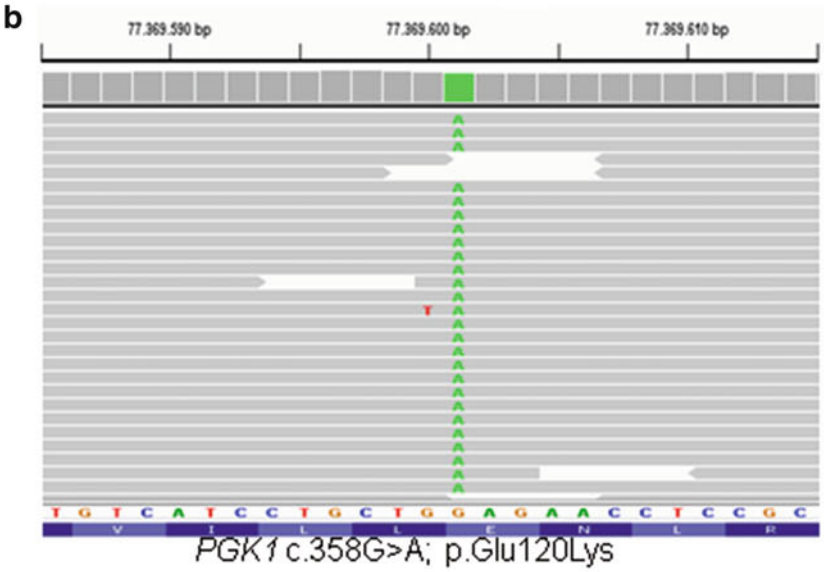
b
77.369.590 bp
77.369.600 bp
77.369.610 bp
PGK1 c.358G>A; p.Glu120Lys

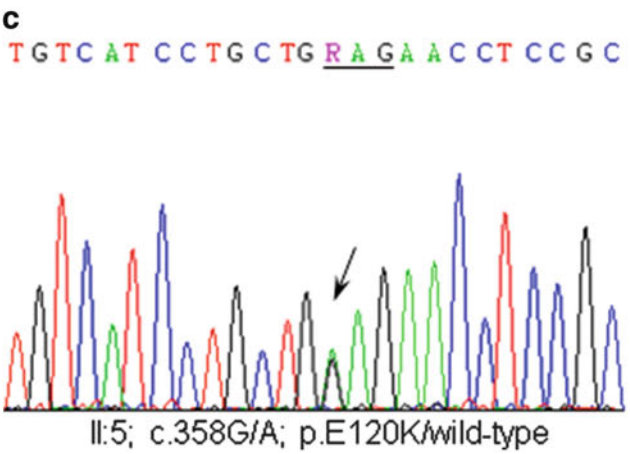
c
TGTCATCCTGCTGRAGAACCTCCGC
II:5; c.358G/A; p.E120K/wild-type

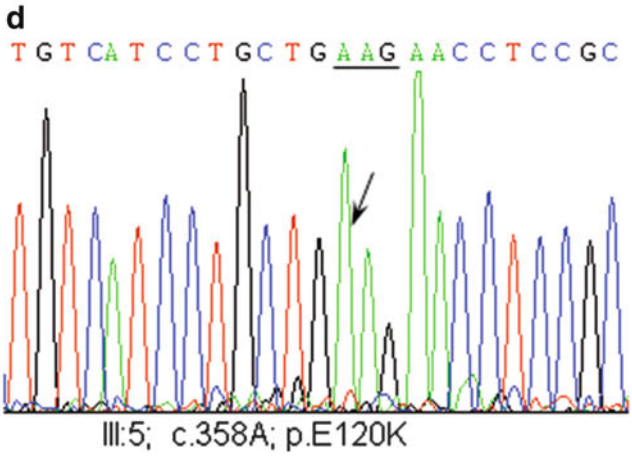
d
TGTCATCCTGCTGAAGAACCTCCGC
III:5; c.358A; p.E120K

Table 1 Clinical features in subject carriers of either the *PGK1* c.358A mutation or the t(3;14) translocation alone or in association

Clinical features	III:2 PGK1 c.358A	III:4 PGK1 c.358A&t(3;14)	III:5 PGK1 c.358A&t(3;14)	III:3 t(3;14)	NUBPL [a]252010	CCDC39 [a]613807	DNAJC19 [a]610198
Hemolytic anemia	Severe	Severe	Severe	No	NR	NR	Normochromic microcytic
Erythroblastosis fetalis	Yes	Yes	Yes	No	–	–	NR
Jaundice	Yes	Yes	Yes	No	–	–	NR
Hyperbilirubinemia	Yes	Yes	Yes	No	–	–	NR
Hemolytic crisis	Severe	Severe	Severe	No	–	–	NR
Hepatosplenomegaly	Yes	Yes	Yes	No	–	–	NR
Splenectomy	ND	No	Yes	No	–	–	NR
Hemoglobin	Decreased	Decreased	Decreased	No	–	–	NR
MCV	Normal	Decreased	Decreased	No	–	–	Decreased
Neurological dysfunction	Yes	Yes	Yes	No	Characteristic	NR	Described
Neonatal hypotonia	No	Yes	Yes	No	–	–	NR
Developmental delay	Moderate	Yes	Yes	No	Characteristic	–	Described
Intellectual disability	Mild	Severe	Severe	No	Described	–	Described
Speech	Delayed	Absent	Absent	Normal	Described	–	Reported
Seizures, epilepsy	Severe	Severe	Severe	No	Reported	–	NR
Encephalopathy	Yes	Yes	Yes	No	Described	–	NR
Ataxia	NR	NR	NR	Transient	Described	–	Reported
Myopathy	Yes	Yes	Yes	No	Characteristic	NR	Cardiomyopathy
Muscular dystrophy	No	Severe	Severe	No	–	–	–
Weakness	Yes	Yes	Yes	Yes	Yes	–	Yes
Unsupported walking	Walk with help	Never sit or walk	Never walked	No	Characteristic	–	Characteristic
Spastic muscular tone	Yes	Yes	Yes	No	Described	–	–
Nuchal and dorsal muscle hypotonia	Yes	Yes	Yes	No	–	–	–
Swallow, tube feeding	Yes	Yes	Yes	No	Described	–	–
Horizontal nystagmus	Unknown	Yes	Yes	No	Characteristic	–	Reported
Infection	Repeated	Repeated	Repeated	No	–	Characteristic	–

[a] OMIM number
NR not reported (see also Table S2)

The 3q26.33 breakpoint is at position g.180,278,286_180,278,294delTTCTGCA, 41.6 kb upstream of the 5′ region of tetratricopeptide repeat domain 14 (*TTC14*), a gene whose function is presently unknown (Fig. S3). Additional genes localized further distal from the breakpoint are (1) the coiled-coil domain containing 39 (*CCDC39*) localized only at 53.5 kb, (2) the *FXR1*, and (3) the DnaJ (Hsp40) homologue, subfamily C, member 19 (*DNAJC19*). This gene encodes an important protein for mitochondrial physiology. Located at the inner mitochondrial membrane, it has been shown to function as a chaperone for mitochondrial protein import system. Defects in this gene are reported to cause an autosomal recessive secondary 3-methylglutaconic aciduria (OMIM #610198), a disorder that partially overlaps with that of reported subjects (Table 1) (Wortmann et al. 2012, 2013;

Fig. 1 (continued) Pedigree of the family, WES, and confirmation of the X-linked *PGK1* c.358G>A, p.E120K mutation. (**a**) Pedigree illustrating the segregation of the t(3;14)(q26.3;q12) and *PGK1* mutation. The index patient is indicated by *asterisk*. Translocation carriers are shown as hatched or half-hatched symbols, whereas filled and half-filled symbols denote the segregation of *PGK1* mutation. Data in parentheses are inferred. The ratio of X-chromosome inactivation of PGK1 mutation carrier females is indicated (Xa: active X chromosome). (**b**) Alignment of WES reads visualized using IGV tool indicating the homozygous single base substitution in exon 4 of *PGK1*. (**c**, **d**) Confirmation of the missense mutation c.358G>A; p.E120K by Sanger sequencing in subjects II:5 and III:5

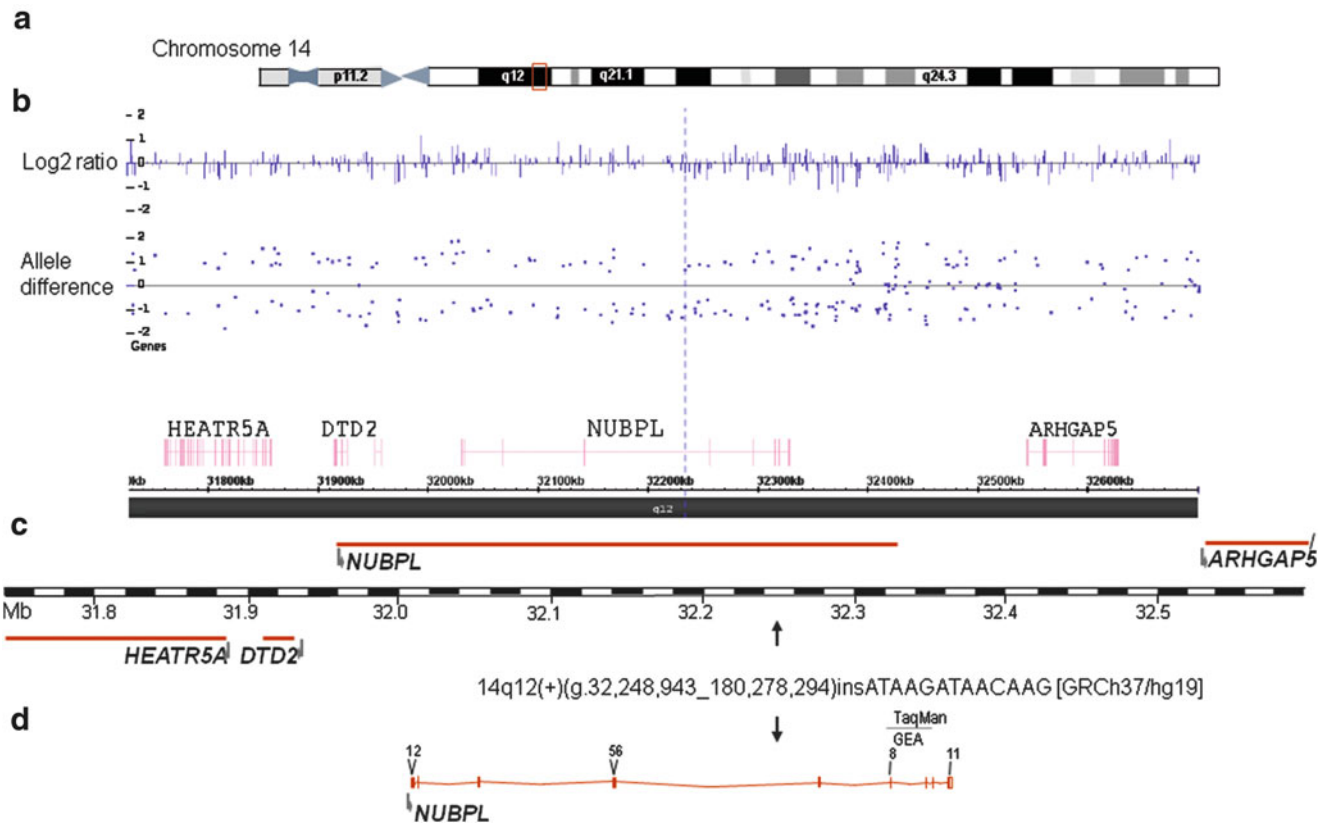

Fig. 2 Overview of the chromosome 14q12 breakpoint region. (**a**) Schematic ideogram of chromosome 14; the breakpoint region is highlighted by a *box*. (**b**) Array analysis of the 14q12 breakpoint region using the Genome-Wide Human SNP array 6.0. A *dashed line* highlights the position of the breakpoint; Log2 ratios and allele differences are shown from the region (each *dot point* represents an oligonucleotide probe). Below, genes within this interval are depicted. No genomic imbalance can be identified within this region. (**c**) Detailed physical map across the breakpoint region. *Horizontal lines with folded gray arrows* indicate the position of genes in sense (above the map) and antisense (below the map) orientation. (**d**) Detailed map of *NUBPL* (RefSeq NM_025152.2) indicating the position of breakpoint at nucleotide resolution and the positions of TaqMan gene expression assay probe

Davey et al. 2006). Therefore, serum and urine amino acid and urine organic acid levels were determined (see Table S3A and S3B). In subject III:3, 3-hydroxybutyric acid was especially increased, but also 3-methylglutaconic acid (3-MGA) and 3-methylglutaric acid (3-MG) were slightly increased.

The 14q12 breakpoint is at position g.32,248,943_32,248,944dupATAAGATAACAAG, within IVS6 of *NUBPL* (Fig. 2), a member of the Mrp/NBP35 ATP-binding protein family, and critical for the assembly of human respiratory mitochondrial CI (Sheftel et al. 2009). Recently, recessive mutations in *NUBPL* have been implicated in the genetic etiology of CI deficiency [OMIM #252010], a mitochondrial respiratory chain defect that is caused by mutations in multiple different nuclear, mitochondrial, or X-linked genes (Calvo et al. 2010; Fassone and Rahman 2012). Additionally, in subjects with pediatric neurological disorders, three deletions encompassing this gene were reported ($p = 0.135$) (Cooper et al. 2011).

Exclusion of Genomic Imbalance and Identification of the Additional Genetic Defect

Pathogenic genomic imbalance that could explain the phenotypic inconsistency observed among translocation carriers was excluded by SNP 6.0 array analysis.

Subsequently, reevaluation of the family history revealed that the maternal cousin (III:2; Fig. 1a) presented a clinical phenotype resembling that of index subject. Based on this, two possible disorders, X-linked PGK1 and triosephosphate isomerase 1 (*TPI1*; OMIM #190450, 12p13.31) deficiencies, were suggested. Furthermore, X-chromosome segregation analysis among siblings using array-based SNP data corroborated the possibility of PGK1 deficiency (data not shown).

Consequently, WES of the index subject revealed a novel missense mutation c.358G>A that leads to a change from glutamic acid to lysine at position 120 of PGK1 (p.E120K) within exon 4 (Fig. 1b). Segregation study confirmed this alteration in the index subject and showed that female subjects I:2, II:3, and II:5 are asymptomatic carriers (Fig. 1a, c and d), whereas the remaining family members are normal. Substitution of the highly conserved, solvent-exposed, negatively charged glutamic acid 120 by positively charged lysine (E120K; Table S7, Figs. S4 and S7) increases the net charge of the protein by two units (from 2.8 to 4.8 at pH 7.4) and certainly strongly argues in favor of this being the disease-causing mutation.

Borderline skewed X-chromosome inactivation toward the normal allele (25:75) was observed in female II:5, the only mutation carrier that presented symptoms during pregnancy (data not shown).

Functional Characterization of the PGK1 p.E120K Variant

The specific activity of the purified PGK1-E120K variant was 10.2 U/mg compared to that of 816 U/mg of PGK1-WT (Chiarelli et al. 2012).

Kinetic analysis showed that, like PGK1-WT, PGK1-E120K variant was activated by high substrate concentrations (Fig. 3a and b) (Chiarelli et al. 2012). The mutant enzyme turned out to be severely affected in its kinetic properties (Table S4), showing a reduction of two orders of magnitude of its apparent k_{cat} values toward both substrates. The apparent K_m value toward 3-PG was sevenfold increased with respect to that of PGK1-WT, whereas that toward Mg-ATP was practically unchanged.

Interestingly, the variant's thermal inactivation rate curve was biphasic, with an increased slope after 5 min incubation, suggesting that it underwent heat-induced molecular change leading to the loss of enzyme activity (Fig. S5).

Gene Expression Studies

Expression array profiling of LCLs from translocation carriers (only one of them affected by the *PGK1* mutation) did not reveal significantly altered expression of genes from the breakpoints (Table S5). The expression level of the disrupted *NUBPL* was only reduced by ~1 SD.

Subsequently, expression levels of three of these genes were also analyzed in subjects II:5, III:5, III:3, III:6, and controls by RT-qPCR (Fig. 4a, Table S5, Fig. S6A and B). By this analysis, a statistically significant 2.6-fold reduction of the *NUBPL* expression level ($P = 0.0001$; 0.061 vs. 0.156) was observed.

Additionally, systematic analysis of array expression data of mitochondrial CI subunits did not show considerable alteration in their expression (Table S6).

SDS-PAGE Western Blot Analysis

Levels of the five OXPHOS complexes as well as the NUBPL assembly factor were determined by SDS-PAGE Western blot in LCLs, as our attempt to establish a fibroblast cell line from the index subject was unsuccessful.

NUBPL levels were reduced in all translocation carriers although at different extent (Fig. 4b). No significant changes were observed in the levels of the five complexes

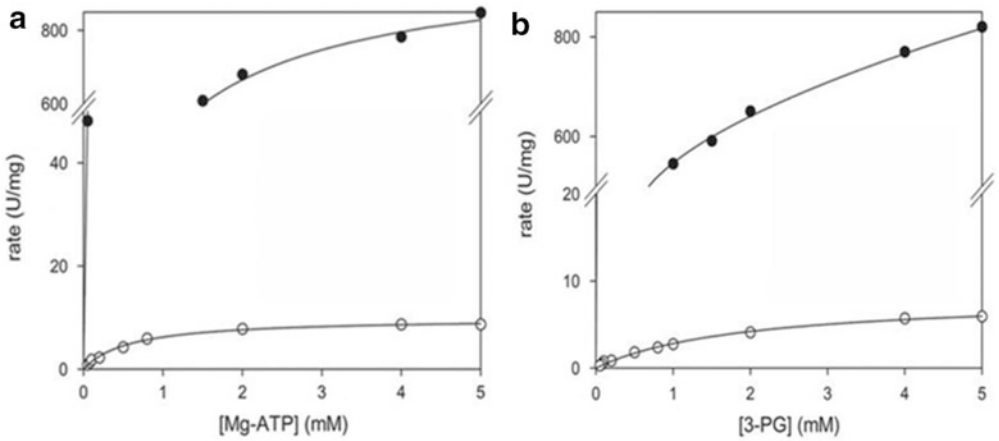

Fig. 3 Kinetic profile of PGK1-E120K variant vs. wild-type enzyme. Steady-state kinetics of PGK1-E120K variant and wild-type as function of (**a**) Mg-ATP at fixed 5 mM 3-PG concentration and (**b**) as of 3-PG at fixed 5 mM Mg-ATP concentration. *Open circles* represent the PGK1-E120K variant, whereas filled circles represent the wild type. Like the wild type, the PGK1-E120K variant presents a biphasic kinetic behavior toward the two substrates; therefore, the linear region (0–5 mM substrates, range of physiological concentration) was considered to extrapolate the kinetic parameters

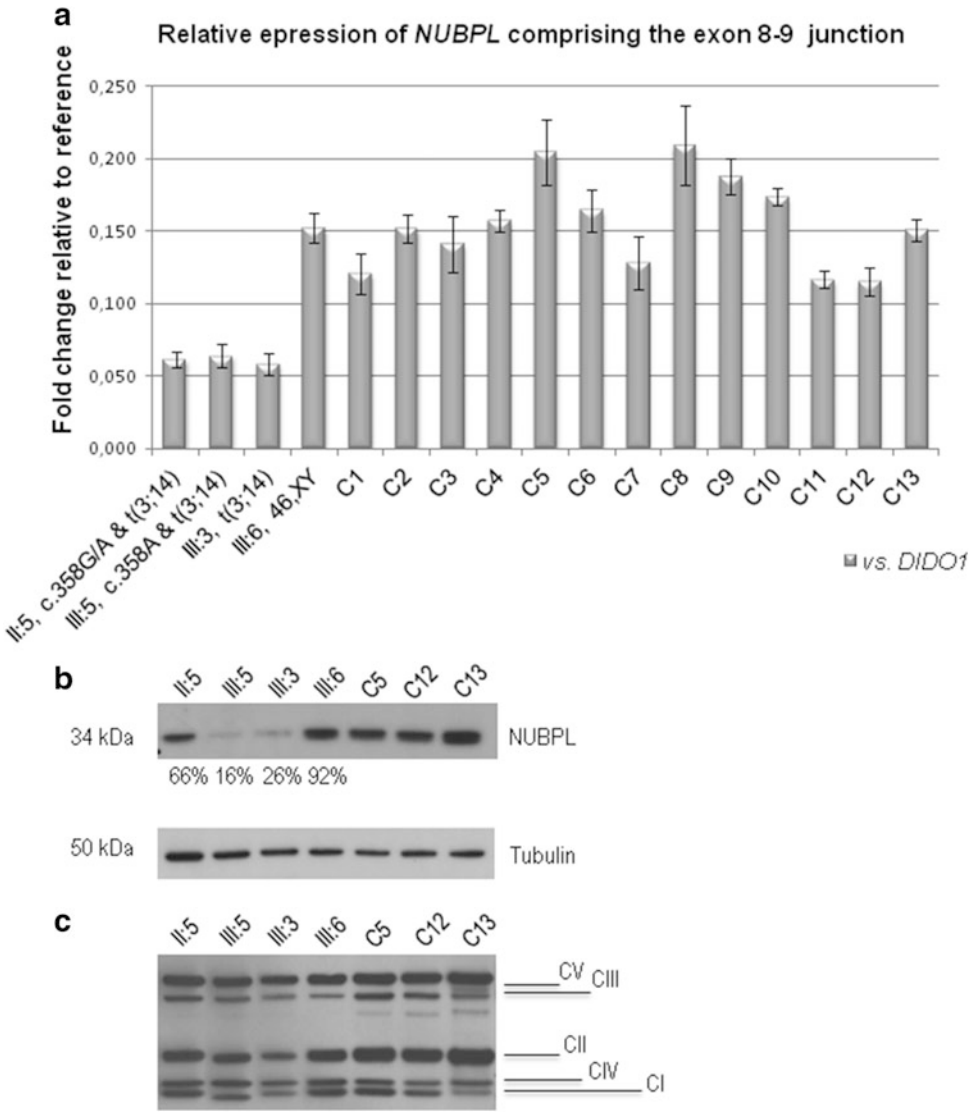

Fig. 4 Quantification of *NUBPL* mRNA and protein in LCLs of translocation carriers and controls. (**a**) Bar graph depicting the relative expression of the *NUBPL* transcript comprising the exon 8–9 junction. Expression levels were normalized to the internal control (*DIDO1*). Fold change relative to reference is given in 2ΔCt. *Error bars* represent standard deviation, and C1 to C13 are control LCLs from unrelated subjects. (**b**) SDS-PAGE Western blot of NUBPL and alpha tubulin (loading control) in the family members and control LCLs showing significant reduction of NUBPL in the individuals affected by the translocation. NUBPL expression levels were normalized to the loading control. (**c**) SDS-PAGE Western blot of MitoProfile Total OXPHOS Human WB antibody cocktail

by the OXPHOS antibody cocktail (Fig. 4c). The dissimilar reduction of NUBPL protein in translocation carriers is in striking contrast with the evenly reduced mRNAs levels (Fig. 4a).

Discussion

Alleged association of the familial translocation t(3;14) (q26;q12) with a particularly severe hemolytic anemia and neuromyopathy led us to map the translocation breakpoints, at nucleotide resolution.

Given the absence of genomic imbalance that could explain the phenotypic inconsistency observed among translocation carriers, and taking into account previously unreported family medical history data, the presence of an additional genetic defect was hypothesized. Segregation analysis of X chromosome and WES revealed that the index subject is also affected by a novel X-linked *PGK1* mutation (c.358G>A, p.E120K) within a highly conserved region.

Biochemical and functional characterization of the PGK1-E120K variant showed highly perturbed kinetic properties (Table S4). Very likely the p.E120K substitution

leads to a distorted local protein structure with detrimental indirect effect on the active site geometry, locking the enzyme in a more tight conformation and hindering proper domain movements required for its catalytic activity. Additionally, the variant turned out to have weakened protein stability (Fig. S4) most likely due to an intrinsic propensity of aggregating in a temperature- and time-dependent manner (Pey et al. 2013). These data led us to conclude that p.E120K is one of the most severely impaired PGK1 variants characterized thus far (Fermo et al. 2012; Chiarelli et al. 2012) and consequently the main genetic cause of the phenotype observed in this family.

Although rare, lethal forms of PGK1 deficiency during infancy have been reported in the literature (Beutler 2007). Even more infrequent are PGK1-deficient patients exhibiting the three distinguishing clinical features of this deficiency (hereditary non-spherocytic hemolytic anemia, neurological dysfunction, and myopathy). In the family reported here, all affected subjects (III:2, III:4, and III:5) presented the full clinical spectrum of PGK1 deficiency, and seemingly they are among the most severely affected PGK1-deficient patients reported to date.

The disruption of *NUBPL* by the 14q12 breakpoint led to a 60% reduction of the mRNA expression level of this CI assembly factor in three family members. Concomitant reduction of the protein level was also observed, being the index subject, the most affected one. The translocation per se is only associated with a subclinical state as the only clinical feature reported in translocation carriers (without PGK1 deficiency) is exercise intolerance due to premature fatigue, a common symptom of mitochondrial myopathy.

Interestingly, homozygous subjects for the branch-site mutation c.815-27T>C within IVS 9 of *NUBPL* are predicted to have ~30% of NUBPL expression. This mutation was excluded in the presently reported family (data not shown). The partially impaired CI function in these subjects is also sub-pathologic and certainly not associated to a mitochondrial CI disease (Tucker et al. 2012).

Although generally the clinical phenotype of family members carrying identical PGK1 mutations is reportedly similar, both translocation carriers (III:4 and III:5), unlike their translocation noncarrier cousin, show severe neuromyopathy with exacerbated muscular dystrophy.

In different tissues or pathogenic conditions, one of the two metabolic pathways, glycolysis or OXPHOS, is predominant over the other (Hu et al. 2012). Additionally, these pathways are interconnected as cytosolic NADH, the electron supplier that drives ATP synthesis via OXPHOS, is generated through glycolysis to pyruvate by glyceraldehyde-3-phosphate dehydrogenase (GAPDH) [see Glycolysis: Regulating Blood Glucose, http://themedicalbiochemistry-page.org/glycolysis.php] (Ramzan et al. 2013). Synergistic interactions, called synergistic heterozygosity, between defects in one or more different energy metabolism pathways have been reported as a common disease mechanism (Vockley et al. 2000). Such interaction between the reported genetic defects, both participating in cellular energy metabolism, seems obvious.

Although unlikely, we cannot exclude that other genes from the breakpoint regions, such as *DNAJC19*, may also contribute to the increased clinical severity of PGK1 deficiency in translocation carriers. The slight increase of both 3-MGA and 3-MG observed in the index subject can be related with several features of the clinical phenotype (metabolic disorder, mitochondrial dysfunction, progressive neuromuscular degeneration, and anemia) (Wortmann et al. 2013). Additionally, glycogen granules and granular structures in the mitochondria of endothelial cells and muscle fibers were reported in a PGK1-deficient subject (Schröder et al. 1996). Therefore, involvement of PGK1 deficiency in mitochondrial dysfunction seems likely and can also be related to the drastic reduction of NUBPL in the index subject.

Even more unlikely, but theoretically possible, is that the observed phenotype is exclusively the result of the novel PGK1 mutation, and the phenotype heterogeneity observed among translocation carriers and noncarriers is the outcome of each individual's genomic/epigenetic background.

In conclusion, the discordant inheritance of the allegedly translocation-associated severe phenotype, instead of being due to a genomic imbalance, is mainly explained by independent inheritance of a novel *PGK1* c.358G>A, p.E120K mutation. The pathogenicity of this mutation was confirmed by in vitro functional characterization of the variant. Furthermore, the t(3;14)(q26;q12) is only associated with a subclinical phenotype; nevertheless, disruption NUBPL, a component of the OXPHOS cellular energy pathway, most likely exacerbates the PGK1-deficient phenotype in subjects who are also translocation carriers. In addition, the case presented here constitutes a "beautiful" example of synergistic heterozygosity and a naturally occurring model to study the interactions between cellular energy pathways and their association with mitochondrial dysfunction. Therefore, further studies are warranted to clarify these additional aspects.

Additionally our data imply that synergistic interactions, involving heterozygous genomic and chromosome rearrangements, may contribute for the "missing" heritability

of inborn metabolic disorders. Last but not least, this study eloquently illustrates that even in our genomic era with WES and personalized genomics, a thorough family medical history is necessary in the elucidation of the molecular bases of rare diseases and their prevention.

Acknowledgments We are grateful to the family members and the referring physician, Matild Dobos, for their involvement in this study. We thank the Chrombios Molecular Cytogenetics GmbH (Raubling, Germany), the Gulbenkian Institute of Sciences (Oeiras, Portugal), and the DNAVision (Gosselies, Belgium) for carrying out chromosome sorting and processing Affymetrix SNP 6.0 arrays and WES, respectively. Additionally, we would like to thank Sara Malveiro for the technical support at the beginning of this work, to Catarina Fernandes for the segregation analysis of the novel PGK1 mutation, and to Barbara Marques for the fluorescence in situ hybridization (FISH). We are also grateful to Andreas Gal and João Lavinha for their comments on the manuscript.

Funding: C.A. was supported by the Ricardo Jorge Research Fellowship (BRJ/01/DG/2009) from the *Instituto Nacional de Saúde Dr Ricardo Jorge*. L.S.A is supported by the Portuguese Foundation for Science and Technology (FCT) fellowship (C2008/INSA/P4). This work was partially supported by FCT research grants PTDC/SAU-GMG/118140/2010 and PEst-OE/SAU/UI0009/2011 as well as by a Portuguese-Hungarian bilateral collaboration grant.

Synopsis

An extremely severe non-spherocytic hemolytic anemia and neuromyopathy, hypothesized to be associated with chromosome translocation-associated genomic imbalance, were shown to be mainly caused by a novel pathogenic severe *PGK1* mutation and that the neuromyopathic symptoms of the deficiency are likely exacerbated by the disruption of mitochondrial complex I assembly factor, NUBPL.

Compliance with Ethics Guidelines

Conflict of Interest

Dezső David, Lígia S. Almeida, Maristella Maggi, Carlos Araújo, Stefan Imreh, Giovanna Valentini, György Fekete, and Irén Haltrich declare that they have no conflict of interest.

Informed Consent

All procedures followed were in accordance with the ethical standards of the responsible committee on human experimentation (institutional and national) and with the Helsinki Declaration of 1975, as revised in 2000.

Informed consent was obtained from all subjects for being included in the study.

Additional informed consent was obtained for the patient for which identifying information (photograph) is included in this article.

Details of the Contributions of Individual Authors

DD designed, oriented, and analyzed the results and wrote the manuscript, LSA performed immunodetection of NUBPL, MM and GV performed in vitro characterization of the PGK1 variant, CA carried out RT-qPCR and sequencing of the junction fragments, SI contributed to the WES, and GF and IH contributed with identification, clinical description, and samples from family members. All authors contributed to the manuscript.

References

Beutler E (2007) PGK deficiency. Br J Haematol 136:3–11

Calvo SE, Tucker EJ, Compton AG et al (2010) High-throughput, pooled sequencing identifies mutations in NUBPL and FOXRED1 in human complex I deficiency. Nat Genet 42: 851–858

Chiarelli LR, Morera SM, Bianchi P, Fermo E, Zanella A, Galizzi A, Valentini G (2012) Molecular insights on pathogenic effects of mutations causing phosphoglycerate kinase deficiency. PLoS One 7:e32065

Cooper GM, Coe BP, Girirajan S (2011) A copy number variation morbidity map of developmental delay. Nat Genet 43:838–846

Davey KM, Parboosingh JS, McLeod DR et al (2006) Mutation of DNAJC19, a human homologue of yeast inner mitochondrial membrane co-chaperones, causes DCMA syndrome, a novel autosomal recessive Barth syndrome-like condition. J Med Genet 43:385–393

David D, Marques B, Ferreira C, Vieira P, Corona-Rivera A, Ferreira JC, van Bokhoven H (2009) Characterization of two ectrodactyly-associated translocation breakpoints separated by 2.5 Mb on chromosome 2q14.1-q14.2. Eur J Hum Genet 17:1024–1033

David D, Marques B, Ferreira C et al (2013) A familial t(8;13) translocation associated TRPS I and a novel expanded TRP syndrome most likely caused by cis-ruption and increased *TRPS1* expression. Hum Genet 132:1287–1299

De Gregori M, Ciccone R, Magini P et al (2007) Cryptic deletions are a common finding in "balanced" reciprocal and complex chromosome rearrangements: a study of 59 patients. J Med Genet 44: 750–762

Fassone E, Rahman S (2012) Complex I deficiency: clinical features, biochemistry and molecular genetics. J Med Genet 49: 578–590

Fermo E, Bianchi P, Chiarelli LR et al (2012) A new variant of phosphoglycerate kinase deficiency (p.I371K) with multiple tissue involvement: molecular and functional characterization. Mol Genet Metab 106:455–461

Hu Y, Lu W, Chen G et al (2012) K-rasG12V transformation leads to mitochondrial dysfunction and a metabolic switch from oxidative phosphorylation to glycolysis. Cell Res 22:399–412

Kevelam SH, Rodenburg RJ, Wolf NI et al (2013) NUBPL mutations in patients with complex I deficiency and a distinct MRI pattern. Neurology 80:1577–1583

Pey AL, Mesa-Torres N, Chiarelli LR, Valentini G (2013) Structural and energetic basis of protein kinetic destabilization in human phosphoglycerate kinase 1 deficiency. Biochemistry 52: 1160–1170

Ramzan R, Weber P, Linne U, Vogt S (2013) GAPDH: the missing link between glycolysis and mitochondrial oxidative phosphorylation? Biochem Soc Trans 41:1294–1297

Schäffer AA (2013) Digenic inheritance in medical genetics. J Med Genet 50:641–652

Schröder JM, Dodel R, Weis J, Stefanidis I, Reichmann H (1996) Mitochondrial changes in muscle phosphoglycerate kinase deficiency. Clin Neuropathol 15:34–40

Sheftel AD, Stehling O, Pierik AJ et al (2009) Human Ind1, an iron-sulfur cluster assembly factor for respiratory complex I. Mol Cell Biol 29:6059–6073

Tamai M, Kawano T, Saito R, Sakurai et al (2014) Phosphoglycerate kinase deficiency due to a novel mutation (c. 1180A>G) manifesting as chronic hemolytic anemia in a Japanese boy. Int J Hematol 100:393–397

Tucker EJ, Mimaki M, Compton AG, McKenzie M, Ryan MT, Thorburn DR (2012) Next-generation sequencing in molecular diagnosis: NUBPL mutations highlight the challenges of variant detection and interpretation. Hum Mutat 33:411–418

Vockley J, Rinaldo P, Bennett MJ, Matern D, Vladutiu GD (2000) Synergistic heterozygosity: disease resulting from multiple partial defects in one or more metabolic pathways. Mol Genet Metab 71: 10–18

Wortmann SB, Kluijtmans LA, Engelke UFH et al (2012) The 3-methylglutaconic acidurias: what's new? J Inherit Metab Dis 35: 13–22

Wortmann SB, Kluijtmans LA, Rodenburg RJ, et al (2013) 3-Methylglutaconic aciduria—lessons from 50 genes and 977 patients. *J Inherit Metab Dis* 36:913–921

Clinical severity of PGK1 deficiency due to a novel p.E120K substitution is exacerbated by co-inheritance of a subclinical translocation t(3;14)(q26.33;q12), disrupting *NUBPL* gene

Dezső David, Lígia S. Almeida, Maristella Maggi, Carlos Araújo, Stefan Imreh, Giovanna Valentini, György Fekete, Irén Haltrich

Dezső David, Lígia S. Almeida, Carlos Araújo Department of Human Genetics, National Institute of Health Dr Ricardo Jorge, Lisbon, Portugal
Maristella Maggi, Giovanna Valentini Department of Biology and Biotechnology "L. Spallanzani", University of Pavia, Pavia, Italy
Maristella Maggi
Department of Molecular Medicine, Unit of Immunology and Pathology, University of Pavia, Pavia, Italy
Stefan Imreh Microbiology and Tumour Biology Center, Karolinska Institute, Stockholm, Sweden
György Fekete, Irén Haltrich II Department of Pediatrics, Semmelweis University, Budapest, Hungary

Supplementary Material

Materials and methods

Analysis of WES, *amplification* and segregation analysis of the *PGK1* mutation

Mapping of the sequence reads was carried out by the Burrows-Wheeler Alignment tool (BWA) (Li and Durbin, 2009). For identification of single-nucleotide variants (SNVs) and small insertions / deletions the BWA alignment output SAM file (Sequence Alignment/Map) was further analyzed by SAMtools software package (Li et al, 2009).

Amplification of *PGK1* (RefSeq NM_000291.3) exon 4 from genomic DNAs was carried out using primers described in Table S1.

Confirmation of the novel *PGK1* mutation identified by WES and segregation analysis in available family members was performed by Sanger sequencing as described earlier (David et al, 2009).

X-chromosome inactivation assay

X-chromosome inactivation patterns in female carriers of the PGK1 mutation were assayed according to Kiedrowski and co-workers (Kiedrowski et al, 2011).

Gene expression studies by real-time quantitative PCR (RT-qPCR)

Expression level of three genes from the breakpoint regions were also analyzed using TaqMan gene expression assays. Namely, assay Hs00228512_m1, for exon 8 to 9 junction of

the disrupted *NUBPL*; assay Hs00750732_s1, for exon 2 of Rho GTPase activating protein 5 (*ARHGAP5*) and assay Hs01096865_m1, for exon 2 to 3 junction of fragile X mental retardation, autosomal homolog 1 (*FXR1*). Death inducer-obliterator 1 (*DIDO1*; assay Hs00223101_m1) was used as internal control.

All RT-qPCR reactions were performed in triplicate on an ABI 7000 Sequence Detection System (Applied Biosystems, Foster City, USA). The system's default PCR conditions were used with 40 cycles. Data and statistical analysis were performed as previously described (David et al, 2013).

Expression, purification and characterization of the PGK1-E120K variant

The following mutagenic oligonucleotides were used : 5' CTGTCATCCTGCTGAAGAACCTCCGCTTTC 3' and 5' GAAAGCGGAGGTTCTTCAGCAGGATGACAG 3', respectively (the mutated nucleotides are underlined). The variant cDNA was completely sequenced.

In order to remove protein aggregates, from the purified enzyme variant, a size exclusion chromatographic step on a 16/60 Superdex 75 column (GE Healthcare, Buckinghamshire, UK) equilibrated with 20 mM Tris pH 8.0, 1 mM EDTA, 2mM β-mercaptoethanol, 200 mM NaCl was included (Chiarelli et al, 2012; Pey et al, 2013).

The enzyme activity of PGK1-E120K was measured at 37°C by glyceraldehyde 3-phosphate dehydrogenase (GAPDH)-coupled spectrophotometric assay following the method recommended by the International Committee for Standardization in Hematology (Chiarelli et al, 2012). The standard reaction mixture contained 100 mM Tris pH 8.0, 0.5 mM EDTA, 2 mM MgCl2, 0.24 mM NADH, 0.4 µM GAPDH, 5 mM Mg-ATP and 5 mM 3-phosphoglycerate (3-PG), in a final volume of 0.5 ml. The reaction was started by adding enzyme solution (0.1-0.5 µg).

Kinetic analyses were performed by assaying the enzyme activity at ten different concentrations of 3-PG and Mg-ATP in the presence of 5 mM Mg-ATP and 5 mM 3-PG, respectively. The reaction conditions were identical to those described above. All measurements were performed in triplicate by using a Jasco V-550 UV/VIS spectrophotometer (Jasco, Cremella, Italy). Kinetic parameters were calculated as previously described using SigmaPlot software version 12.0 (IBM SPSS, Inc., Chicago, IL, USA) (Szilágyi and Vas, 1998).

For thermal stability studies, residual enzyme activity was assayed at different time-points after incubation of purified enzyme (0.7 mg/ml) at given temperatures (Chiarelli et al, 2012).

SDS-PAGE and immunodetection

Control and subjects' LCL's pellets were lysed in 200 µl homogenization buffer (150 mM NaCl, 1% NP-40 and 5 mM Tris/HCl, pH 8.0). Equal amounts of protein (15 µg) and a Precision Plus Protein Standards (BioRad, Hercules, CA, USA) were loaded and separated in SDS-PAGE gels (NuPAGE Novex 4-12% Bis-Tris gels; Invitrogen, Carlsbad, CA, USA). Gels were blotted to a PVDF transfer membrane (Immobilion-P, Millipore, Tullagreen, Ireland). Membrane was blocked with 5% skimmed milk and 0.05% Tween-20 in Tris-buffered saline (TBS) for 1 h at room temperature and incubated with primary antibodies, 2h, at room temperature. The following specific antibodies were used: rabbit anti-NUBPL, (Mitosciences, Eugene, OR, USA), mouse anti-tubulin (Sigma, St. Louis, USA) and MitoProfile Total OXPHOS antibody cocktail containing antibodies against: complex I subunit NDUFB8, complex II subunit 30 kDa, complex III subunit Core 2, complex IV subunit II and ATP synthase subunit alpha (Mitosciences, Eugene, OR, USA). Membranes were then washed three times with 0.05% Tween-20 in TBS, incubated with the appropriate

peroxidase-conjugated IgGs secondary antibodies (GE Healthcare) for 1 h at room temperature and developed using Clarity Western ECL Substrate (BioRad). Quantification was performed using the software Quantity One (BioRad).

Results

Clinical reports

Subject III:4 (Fig. 1)

Subject III:4 (Fig. 1A) is the first known affected case in the family, the second (male) child of unrelated, apparently healthy parents. The newborn presented with hepato-splenomegaly and erythroblastosis fetalis, with a mild jaundice that did not require any exchange transfusion. At the end of the first week, generalized spastic muscle tone, nuchal and dorsal muscle hypotonia were observed.

First hospital admission occurred at the age of one and a half months because of severe anemia, requiring blood transfusions. At the age of two months, the following dysmorphic signs were observed: moderate microcephaly, hypertelorism, epicanthal folds, broad nasal bridge, high arched palate, asymmetric face, fronto-occipital cranial elongation, low–set ears, short and pointed nose, frontal bossing, (*see* Table S2). Repeated infections of the respiratory tract, hemolytic episodes and severe general dystrophy during the first year of life made hospital admissions and blood transfusions at every second month necessary. Tonic-clonic seizures occurred for the first time at the age of twenty months. The neurological evaluations led to diagnosis of epilepsy. Increased muscle tone, especially of lower limbs and permanent horizontal nystagmus were obvious. He never sat up or walked and his weight gain stopped. Epileptic seizures became more and more frequent and he had difficulties in swallowing therefore tube feeding was initiated. He died at the age of four and a half years.

Peripheral blood cell analysis revealed low red blood cells (RBC) count (1.9×10^{12}/L), hematocrit (HCT: 0.20) and decreased hemoglobin (61 g/L). Mean corpuscular volume (MCV) was decreased (65μm^3), whereas mean cell hemoglobin (MCH) and mean corpuscular hemoglobin concentration (MCHC) values were in normal range. Reticulocyte count was 98 ‰. Bone marrow contained normal amount of cells with slightly increased erythropoiesis and normal myelopoiesis. Coombs test and hemoglobin electrophoresis, were found as normal. Serum iron, ferritin levels, as well as total iron–binding capacity (TIBC), serum and erythrocyte folate and vitamin B12 levels were as in age-matched controls. Based on shorter erythrocyte lifespan (26 days), decreased osmotic resistance (0.40) and increased permeability, the diagnosis of intrinsic hemolytic anemia was established.

In this period, significant decrease of plasma alkaline phosphatase activity, 10 IU/L, was observed (normal range for child 50-100 IU/L).

Cardiovascular malformation and pathologic meningeal symptoms were not detected. Diagnostic imaging methods did not reveal any structural abnormality of the brain.

Index subject III:5 (Fig. 1)

Blood tests repeatedly showed major increase in creatine phosphokinase (CPK), 60,000 IU/L (normal range for children 50-100 IU/L) as well as of lactate dehydrogenase (LDH), 5,000 U/L, (normal range for children 154-605). At 6 years of age ketogenic diet was initiated.

Cardiac echography and ECG, as well as abdominal ultrasonography resulted in normal findings. No pathologic alteration could be found by audiometric hearing tests. At 11 years of age, sex hormone levels are similar to age-matched prepubertal boys.

Subject III:2 (Fig. 1)

After the parents' informed consent, his hospital records were studied. Indeed, he presented mental retardation, severe hemolytic anemia and seizures. Repeated infections and hemolytic crisis required frequent hospitalization and blood transfusions. At two years of age, he was treated for encephalopathy and liver damage. At six years of age, neurological evaluation was done because of coma and clonic–tonic seizures, resulting in diagnosis of therapy-resistant epilepsy. Owing to swallowing difficulties tube feeding was also initiated from the age of two years. There was a main difference compared to his cousins; he was able to walk with help and he presented generalized edema throughout the whole body. His mother (II:3), although operated because of a thrombotic accident, is healthy. The remaining relatives (I:2, II:1, III:1) are also healthy.

Normal findings have been reported at cardiac examination and echocardiography.

Supplementary Figures

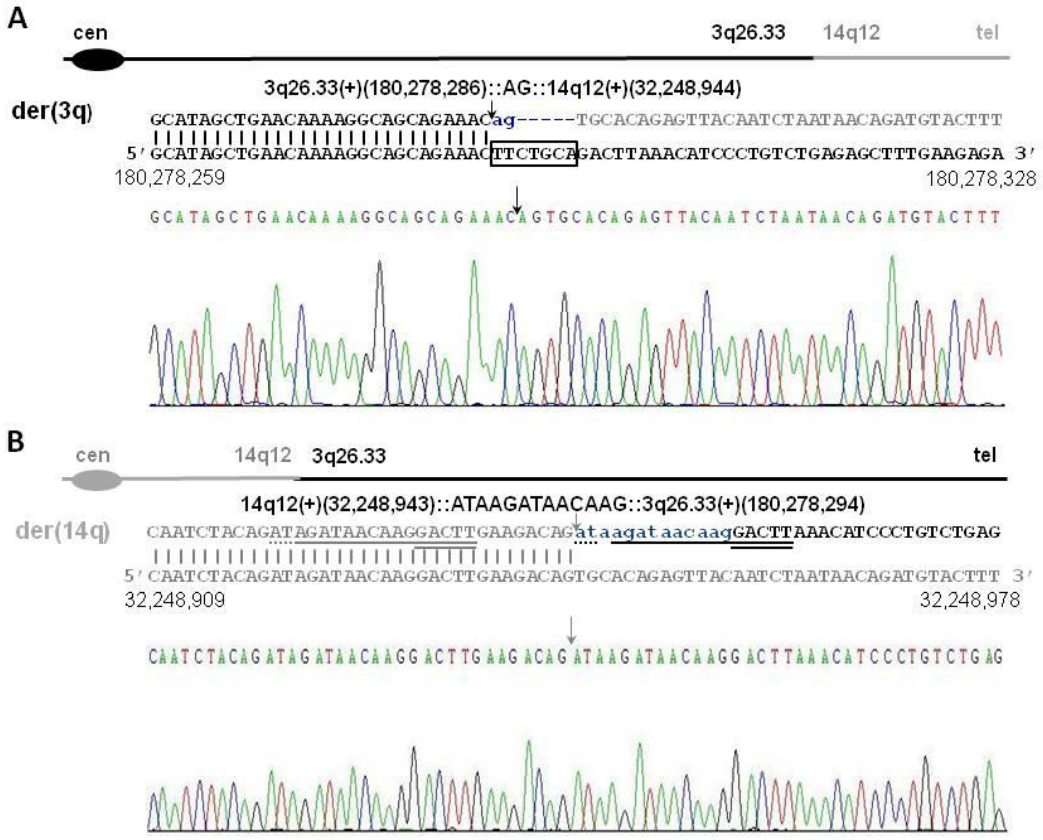

Figure S1. Nucleotide sequence of der(3) and der(14) breakpoints aligned against the reference sequence. (**A**) Derivative chromosome 3 breakpoint. The chromosome 3 sequence is in black, whereas of chromosome 14 in gray. Vertical lines indicate identical nucleotides between derivative and reference chromosomes. The seven nucleotide (TTCTGCT) deletion from the chromosome 3 sequence is boxed, whereas the dinucleotide insertion (AG) at the der(3) breakpoint is in blue lowercase letters. (**B**) Derivative chromosome 14 breakpoint. The a 13 bp duplication (ATAAGATAACAAG) is in blue lowercase letters; the homologous sequence is underlined with solid and dotted lines, whereas those (GACTT) between chromosomes 3 and 14 (GACTT) by double line (reference human genome assembly GRCh37/hg19).

The translocation could be defined as
[GRCh37/hg19]t(3;14)(3pter/3q26(+)(180,278,286)::AG::14q12(+)(32,248,944)14qter;
14pter/14q12(+)(32,248,943)::ATAAGATAACAAG::(+)(180,278,294)/14qter) (Ordulu et al, 2014).

NCBI-GenBank accession numbers of the junction fragment sequences are KJ862055 and KJ862056, respectively.

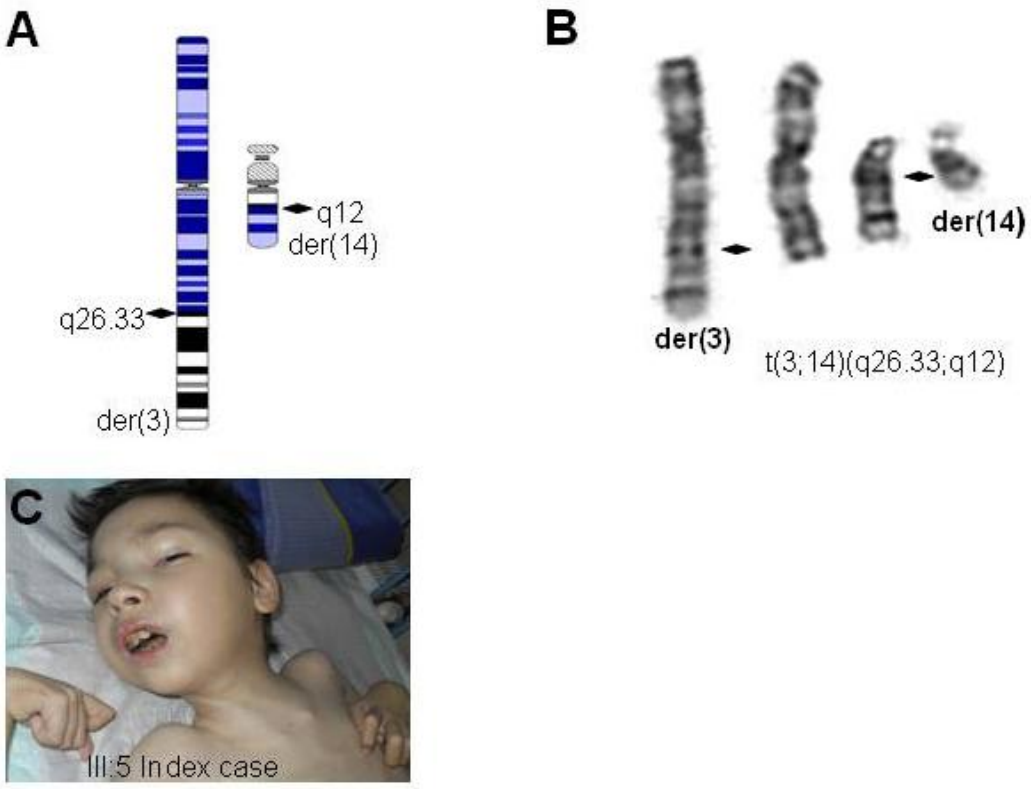

Figure S2. Ideograms, partial karyotype and clinical phenotype of the index subject.
(**A**) Ideograms illustrating the derivative chromosomes. (**B**) Partial karyotype showing the balanced familial translocation t(3;14)(q26.3;q12)] (♦ indicates the chromosome breakpoints). (**C**) Clinical details of the index subject (III:5) - moderate microcephaly, short neck, fronto-occipital cranial elongation, frontal bossing, asymmetric face, hypertelorism, "swimming" eyes, epicanthal folds, broad nasal bridge, short nose, low-set dysplastic ears, total body muscle atrophy, muscle contractures, multiple dental caries **(***see* Table S2**).**

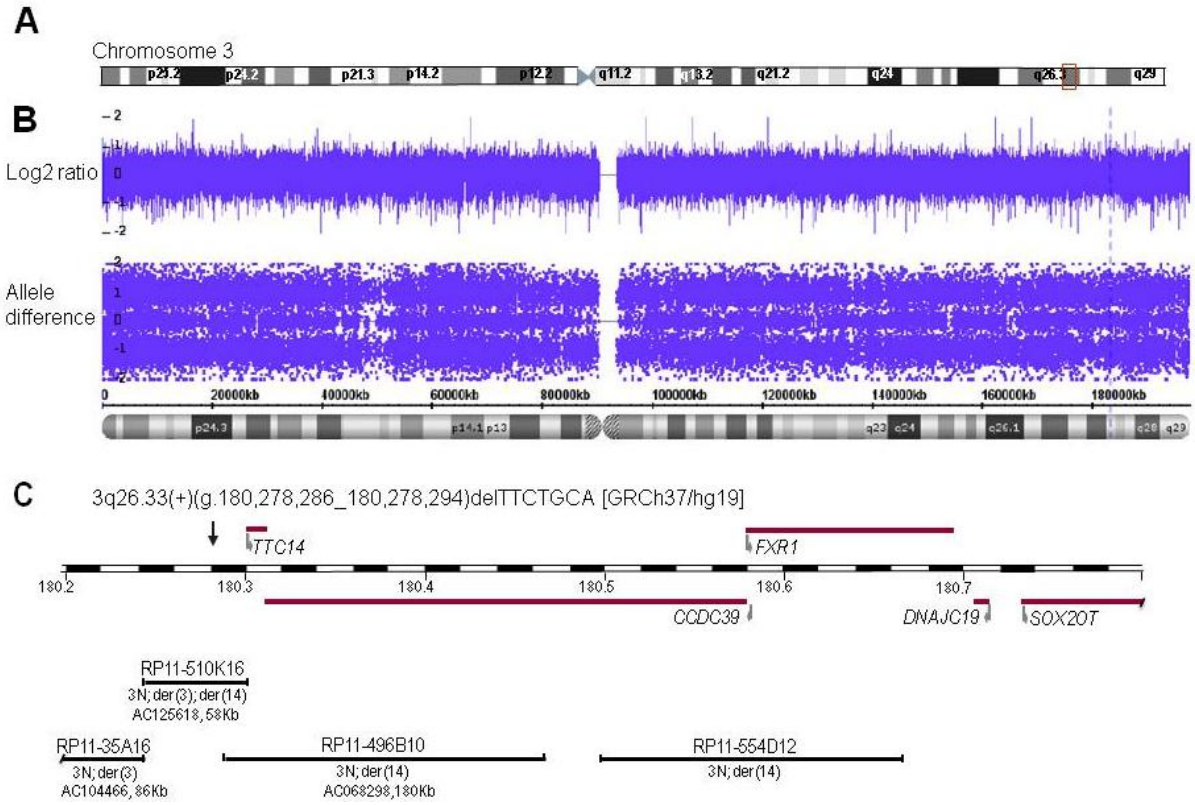

Figure S3. Overview of the chromosome 3 breakpoint region. (**A**) Schematic ideogram of chromosome 3; the breakpoint region is highlighted by a box. (**B**) Array analysis using the Genome-Wild Human SNP array 6.0 from Affymetrix containing 1.8 million markers, (approximately 906,600 SNP and 946,000 copy number probes). Log2 ratios and allele differences are shown indicating the absence of genomic imbalance within this chromosome. (**C**) Detailed physical map across the breakpoint region. Horizontal lines with folded grey arrows indicate the position of genes in sense (above the map) and antisense (below the map) orientation. The position of the breakpoint at nucleotide resolution is specified and indicated by vertical arrow (nomenclature: cytogenetic position of the breakpoint; breakpoint at nucleotide resolution according to the reference chromosome on the positive strand; deleted sequence at the breakpoint; genome reference numbers). Bellow, horizontal lines denote BAC clones used as FISH probes. The hybridization signals and the corresponding GeneBank sequence acc. no. are annotated below the clones.

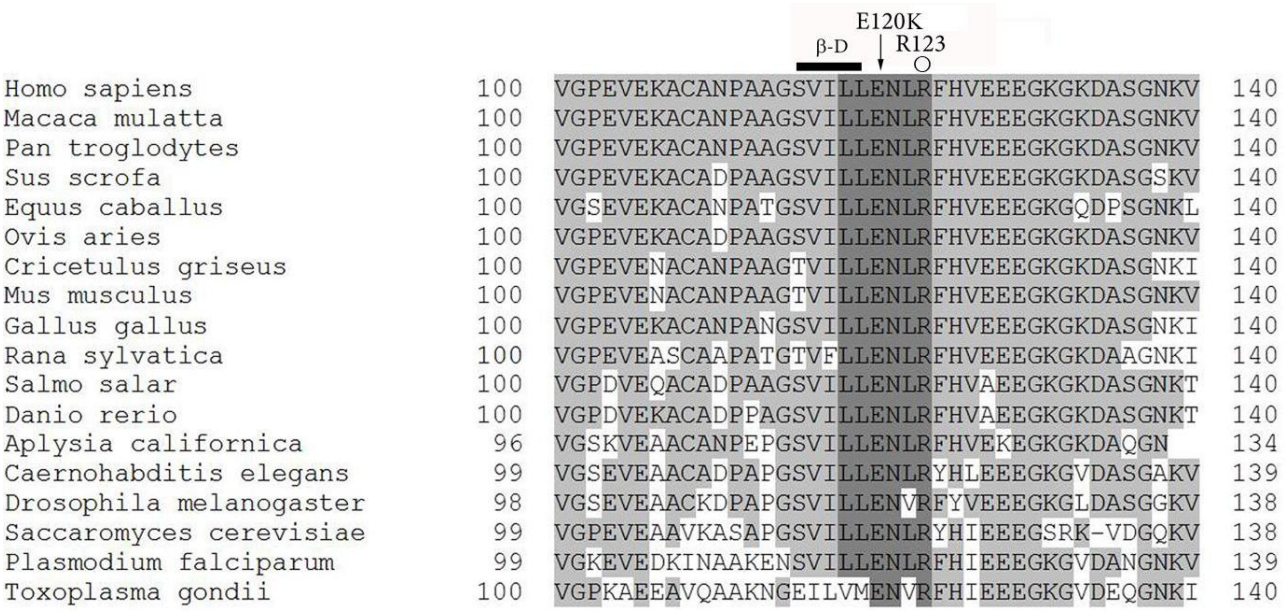

Figure S4. Alignment of the human PGK1 peptide sequence containing the amino acid substitution E120K with corresponding region of PGK from different species. The amino acid numbering of PGK1 starts with methionine. The dark grey zone indicates highly conserved region containing the mutated residue E120K (↓) and the 3-PG substrate binding residue R123 (○), just three amino acids downstream from the mutated one (Vas et al, 2010).
Residue E120 is located on the short loop that follows β-strand D (Fig. S7). Residues belonging to the β-strand D are indicated by the black rectangle.

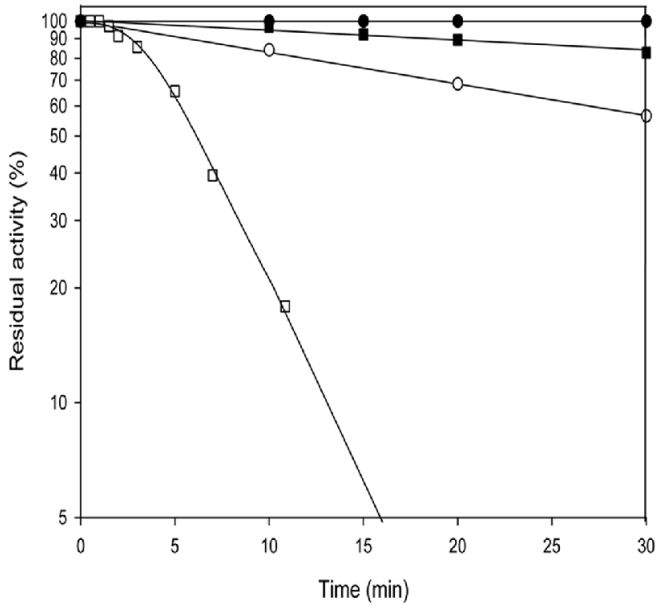

Figure S5. Thermal stability of wild-type and variant PGK1. Heat stability of PGK1-E120K variant (□) at 37°C and 45°C compared to wild-type enzyme (○). Thermal stability was measured by incubating the enzyme (0.7 mg/ml) at the given temperatures in a solution consisting of 20 mM Tris pH 8.0, 1 mM EDTA, 2mM β-mercaptoethanol. Samples (10 µl) were removed at intervals, chilled in ice and immediately assayed according to the published method (Chiarelli et al, 2012). Relative activity was calculated as the percent of the enzyme activity before the incubation. Fill symbols represent data points obtained at 37°C, open symbols at 45°C.

The mutant enzyme lost 50% of its activity after 36 minutes of incubation at 37°C, whereas at 45°C the half time was nearly 6 min.

The variant's thermal inactivation rate at 45°C accounts for an increased heat induced aggregation, as supported by the fact that samples treated at 45°C become more turbid with time. On the other hand, the freshly purified enzyme formed aggregates just after few hours of storage at 4°C.

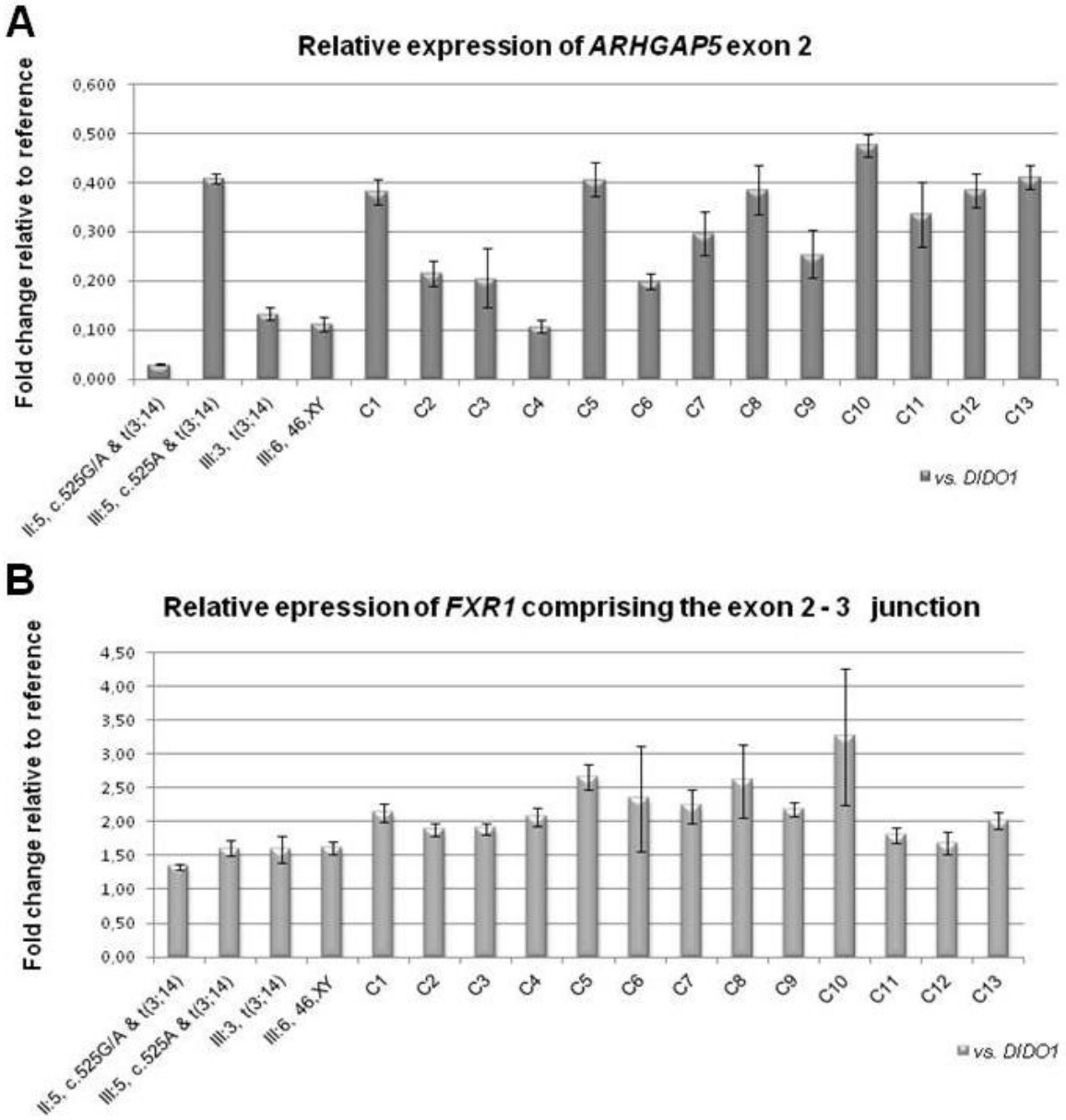

Figure S6. Relative expression levels of two genes from the breakpoint regions in LCLs of family members and controls. (**A**) Bar graph depicting the relative expression of the *ARHGAP5* exon 2 transcript. (**B**) Bar graph depicting the relative expression of the *FXR1* transcript comprising the exon 2-3 junction. Expression levels of both fragments were normalized to the internal control *DIDO1*. Fold change relative to reference is given in 2^{Δ}Ct. Error bars represent standard deviation and C1 to C13 are control LCLs from unrelated subjects.

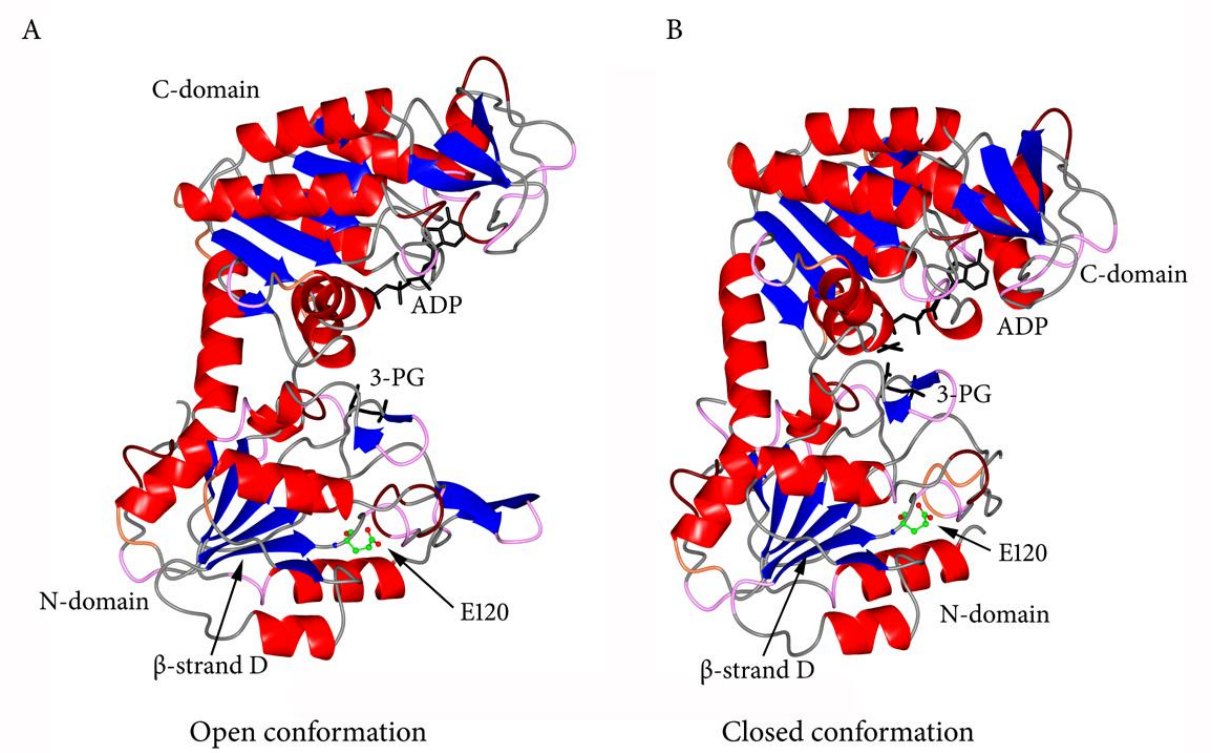

Figure S7. Ribbon representation of the human PGK1 protein structure. Three-dimensional structure of open (**A**, Protein Data Base entry 2XE7) and closed (**B**, Protein Data Base entry 2WZC) human PGK1 associated with Mg-ADP and 3-PG.

PGK1 is a typical hinge-bending monomeric enzyme containing two nearly equal-sized domains, separated by a deep cleft and linked by two α-helices. The N-domain binds 3-PG or 1,3-BPG whereas the C-domain binds Mg-ADP or Mg-ATP. The enzyme can exist in different conformational structures induced by ligands. To perform the catalytic reaction PGK1 has to cycle from an open form to a closed one. The domain closure requires the concerted action of both substrates. The black arrows indicate the E120 amino acid represented as ball and stick and the β-strand D of the N-domain. Residue E120 locates in the loop immediately after the β-strand D and both structural elements are involved in interdomain interactions (Balog et al, 2007). Alpha-helixes are represented as cartoon in red while beta-sheets are in blue; Mg-ADP and 3-PG are shown as black stick models.

Supplementary Tables

Table S1. Primers and amplification conditions used for breakpoint mapping, amplification of junction fragments and of exon 4 of *PGK1*

PCR fragment	Designation	Primer sequence (5'-3')	[a]Primer localization	Annealing *T* (°C)	PCR size (bp)
Junction fragments					
der(3) junction fragment	AC125618-fjF1	TAACATTGAAGATGGCCGAAC	180,277,714-180,277,733	61	787
	AL359400-fjR2	CCAGCTTTTCAGGGAGTGAAT	32,249,156-32,249,136		
der(14) junction fragment	AL359400-fjF1	GCTGGCTTATGATGTGACTTGA	32,248,590-32,248,611	61	862
	AC125618-fjR1	TTCAGCTTTTCTGCTCTGGTTT	180,278,788-180,278,767		
PGK1 exon 4	PGK1Ex4-F	TGGTGCTGGTAGACTTTGTGG	77,369,412-77,369,432	62	379
	PGK1Ex4-R	AAGCTGTGTCGGCATTGTATG	77,369,790-77,369,770		

[a]Numbers indicate the position of the primers in the current genome assembly (GRCh37/hg19).

Table S2. Dysmorphic features in subjects carriers of either the *PGK1* c. 358A mutation or the t(3;14) translocation alone or in association

Clinical features	III:2 PGK1 c.358A	III:4 PGK1 c.358A & t(3;14)	III:5 PGK1 c.358A & t(3;14)	III:3 t(3;14)	NUBPL [a]252010	CCDC39 [a]613807	DNAJC19 [a]610198
Dysmorphic features	no	yes	yes	no	NR	NR	NR
Microcephaly	absent	moderate	moderate	absent	—	—	—
Hypertelorism	unknown	yes	yes	no	—	—	—
Asymmetric face	no	yes	yes	no	—	—	—
Broad nasal bridge	no	yes	yes	no	—	—	—
High arched palate	no	yes	yes	no	—	—	—
Epicanthal folds	unknown	yes	yes	no	—	—	—
Cranial shape	normal	elongated	elongated	normal	—	—	—
Frontal bossing	no	yes	yes	moderate	—	—	—
Low – set ears	no	yes	yes	moderate	—	—	—
Micrognathia	no	yes	yes	moderate	—	—	—
Other							
Genitalia	unknown	phymosis	cryptorchidism	no	—	—	reported
Digital anomalies	no	no	yes	no	—	—	—
Laboratory analyses							
Alkaline phosphatase	unknown	significantly decreased	decreased	no	unknown	—	—
Lactate dehydrogenase (LDH)	increased	increased	increased	no	increased	—	—
Creatine phosphokinase (CPK)	unknown	unknown	increased	normal	unknown	—	—

[a]OMIM number. NR: not reported. Distinctive clinical features are in bold.

NUBPL, OMIM #252010; an autosomal recessive mitochondrial complex I deficiency characterized by: distinctive leukoencephalopathic brain MRI pattern, developmental delay, speech and mobility disability, ataxia, myopathy, nystagmus and absence seizures (Kevelam et al, 2013).

CCDC39, OMIM #613807; an autosomal recessive primary ciliary dyskinesia (PCD) characterized by: neonatal respiratory distress, chronic infections of the respiratory tract, rhinosinusitis, situs inversus, situs ambiguous or Kartagener's syndrome, sperm dysmotility or goasthenospermia and infertility (Antony et al, 2013; Merveille et al, 2011).

DNAJC19, OMIM #610198, 3-methylglutaconic aciduria, type V (MGCA5); an autosomal recessive disorder named dilated cardiomyopathy with ataxia (DCMA) characterized by: increase (5 to 10 fold) in urine 3-methylglutaconic acid (3-MGC) and 3-methylglutaric acid (3-MGA), early-onset dilated cardiomyopathy, long QT syndrome, ECG abnormalities, prenatal or postnatal growth failure, non-progressive cerebellar ataxia causing significant motor delays, testicular dysgenesis, isolated cryptorchidism to severe perineal hypospadias; normochromic microcytic anaemia, mental retardation and increase in hepatic enzymes and liver steatosis (Wortmann et al, 2012).

Table S3A. Serum and urine amino acid concentration

Amino acid	III:5 - PGK1 c. 358A & t(3;14)			III:3 - t(3;14)	III:6 – 46XY	II:5 –mother; PGK1 c.G525A & t(3;14)	Age-matched reference
	Samp1	Samp 2	Samp 3				
Serum concentrations (µmol/l)							
Alanine	260	157	497	393	534	453	155 - 505
Arginine	139	121	138	143	167	140	40 -175
Aspartic acid	**95**	56	**81**	127	142	92	30 - 75
Cysteine	ND	**56**	**35**	ND	ND	ND	<15
Citrulline	**95**	**99**	**75**	42	85	77	25 - 55
Phenylalanine	80	66	58	152	124	91	50 - 130
Glycine	465	328	413	474	651	541	165 - 585
Glutamic acid	190	157	151	176	196	150	70 - 190
Histidine	ND	**289**	**167**	ND	ND	ND	<135
Isoleucine	104	98	49	95	114	61	50 - 90
Leucine	160	113	79	168	191	131	80 - 215
Lysine	312	421	224	255	294	242	95 - 230
Methionine	48	82	33	54	63	47	20 - 45
Ornithine	95	106	93	120	130	100	65 - 180
Tyrosine	82	107	43	85	112	55	45 - 105
Tryptophan	117	186	90	141	166	115	50 - 110
Valine	232	90	114	250	274	204	160 - 315
Ornitine	95	106	93	120	ND	ND	65 - 180
Urine concentrations (nmol/mol creatinine)							
Alanine	259	19.0	ND	17.0	21.0	36.0	10 - 160
Arginine	10.0	7.0	ND	2.0	2.0	2.0	<15
Aspartic acid	**21.0**	**27.0**	ND	2.0	3.0	2.0	<15
Cysteine	**23.0**	**20.0**	ND	9.0	7.0	9,0	<10
Citrulline	10.0	7.0	ND	2.0	2.0	3.0	<8
Phenylalanine	15.0	15.0	ND	11.0	6.0	10.0	<50
Glycine	340.0	201.0	ND	82.0	67.0	181,0	50 - 490
Glutamic acid	**157**	**38.0**	ND	5.0	4.0	3.0	<15
Hydroxyproline	1.0	3.0	ND	0.0	1.0	0,0	<10
Histidine	**379.0**	**219.0**	ND	54.0	125.0	67,0	15 - 180
Isoleucine	**6.0**	**6.0**	ND	2.0	1.0	2.0	<5
Leucine	9.0	18.0	ND	6.0	4.0	5.0	<10
Lysine	42.0	32.0	ND	10.0	11.0	10,0	5 - 50
Methionine	6.0	10.0	ND	1.0	2.0	2,0	<10
Ornithine	8.0	7.0	ND	1.0	1.0	3,0	<12
Proline	**18.0**	**19.0**	ND	3.0	4.0	3,0	<15
Tyrosine	17.0	14.0	ND	11.0	5.0	8,0	5 - 40
Threonine	**95.0**	**114.0**	ND	6.0	8.0	20.0	10 - 75
Tryptophan	**30.0**	**29.0**	ND	9.0	8.0	8.0	>20
Valine	10.0	13.0	ND	3.0	3.0	4.0	>30

Determination of serum and urine amino acid levels was carried out by liquid chromatography / mass spectrometry (LC/MC) using the EZ:Fast amino acid analysis kit (Phenomenex, Torrance, CA, USA).

Samples 1 and 2 of index patient were collected with three months interval during ketogenic diet and sample 3 after suspension of ketogenic diet for 5 days. Age-matched reference values for serum and urine amino acids concentrations were established from healthy children within the age range of 6 to 12 and 8 to16 years, respectively. Amino acid levels in the mother are within the normal range of age-matched controls. Samp: sample; ND: not done.

Table S3B. Urinary organic acid analysis

Organic acids (mmol/mol creatinine)	III:5 PGK1 c.358A & t(3;14)		Age-matched reference	III:3 - t(3;14)	III:6 46,XY	II:5 - mother
	Samp. 1	Samp. 2				
Adipic acid	19.8	25.2	<5.3	0	0	0
Uric acid	32.4	ND	<1.5	0	0	0
Methylmalonic acid	1.5	27.0	0.0	0	0	0
Suberic acid	12.2	16.3	<8.8	0	0	0
3-Hydroxysebacic acid	10.4	20.5	<2.0	0	0	0
3-Hydroxybutyric acid	167.3	1052.2	<7.6	0	0	0
3-Methylglutaconic acid (3-MGA)	21.9	19.0	<11.4	1.0	0	1.6
3-Methylglutaric acid (3-MG)	4.5	2.8	0.0	0.4	1.1	0.5
4-Hydroxyphenyllactic acid	ND	5.0	<3.6	0	0	0
2-Hydroxybutyric acid	ND	14.4	<7.3	0	0	0
3-Hydroxydicarboxylic acid	ND	6.6	0.0	0	0	0

Urinary organic acid profiling was carried out by gas chromatography linked mass spectrometry (GC/MS) methodology after desalting, ethylacetate extraction and oxime-trimethylsilyl derivatization of urine samples.

Samples 1 and 2 were collected with three months interval. Age-matched reference values of healthy children within age range 6 - 12 years. Samp: sample; ND: not done. Levels are expressed in mmol/mol creatinine.

Table S4. Kinetic constants of recombinant PGK1-E120K variant compared to the wild-type enzyme

PGK1 variants	Mg-ATP			3-PG		
	k_{cat} (s^{-1})	K_m (mM)	k_{cat} / K_m (s^{-1} mM^{-1})	k_{cat} (s^{-1})	K_m (mM)	k_{cat} / K_m (s^{-1} mM^{-1})
Wild-type	553.2 ± 28.5	0.28 ± 0.041	1975.7	468.2 ± 33.3	0.17 ± 0.011	2754.1
p.E120K	7.43 ± 0.55	0.59± 0.062	12.59	4.36 ± 0.98	1.18 ± 0,103	3.7

Results are means (± SE) of 3 determinations from at least 3 different protein preparations. Turnover number or k_{cat}, is the number of catalytic events per second, whereas the Michaelis constant or K_m is the substrate concentration at which the reaction velocity is half maximal and k_{cat}/ K_m is a measure of how efficiently an enzyme converts substrate to product at sub-saturating substrate concentrations.

Table S5. Summary of gene expression data obtained by different methods

Gene symbol	Assay	III:3 t(3;14)		III:5 PGK1+t(3;14)		Descriptive statistics			
		NEL	Log2 FC	NEL	Log2 FC	Average	Min	Max	SD
PGK1	HuGene-1.0	12.03	0.002	11.78	-0.190	12.0	11.68	12.31	0.192
3q26.33 region[a]									
USP13	HuGene-1.0	6.72	-0.390	8.13	[c]1.21	7.01	6.56	7.44	0.341
PEX5L	HuGene-1.0	7.63	1.32	5.5	-0.9	6.23	5.16	8.8	1.10
TTC14	HuGene-1.0	9.14	0.412	8.93	0.157	8.76	8.53	9.08	0.172
CCDC39	HuGene-1.0	3.36	-0.096	3.35	-0.08	3.42	3.28	3.68	0.130
FXR1	HuGene-1.0	10.62	-0.099	10.63	-0.01	10.6	10.29	10.89	0.208
	RT-qPCR	NA	1.59	NA	1.60	2.21	1.68	3.25	0.484
DNAJC19	HuGene-1.0	7.29	-0.014	7.28	-0.016	7.28	7.0	7.56	0.176
SOX2	HuGene-1.0	5.25	-0.056	4.78	-0.301	5.23	4.89	5.59	0.229
3q26.33 region[b]									
SCFD1	HuGene-1.0	9.0	-0.241	8.89	-0.391	9.29	8.85	9.72	0.260
COCH	HuGene-1.0	9.35	0.107	9.17	-0.019	9.16	8.21	9.91	0.617
STRN3	HuGene-1.0	9.07	0.056	9.29	0.122	9.08	8.62	9.37	0.242
AP4S1	HuGene-1.0	6.21	0.316	5.55	-0.348	5.92	5.41	6.25	0.342
HECTD1	HuGene-1.0	9.69	0.069	9.63	0.031	9.60	9.32	9.86	0.176
HEATR5A	HuGene-1.0	7.95	0.007	8.04	0.082 0	7.94	6.92	8.93	0.573
DTD2 & C14orf126	HuGene-1.0	9.01	-0.151	9.17	-0.013	916	8.73	9.75	0.281
NUBPL	HuGene-1.0	7.81	-0.160	7.6	-0.292	7.92	7.62	8.31	0.213
	RT-qPCR	NA	[d]0.058	NA	[d]0.064	0.156	0.115	0.209	0.030
ARHGAP5	Array	6.49	[c]-1.54	8.14	0.126	8.03	6.48	8.76	0.706
	RT-qPCR	NA	0.130	NA	0.409	0.312	0.108	0.476	0.108

[a]Expression of genes encompassed within chr3:179357306-182437306 interval; and [b]within chr14:31090249-33050249 interval. [c]Difference greater than 2 SD. The *NUBPL* gene disrupted by the 3q26.33 breakpoint is in bold. [d]Statistically significant reduction.

Table S6. Expression of nuclear complex I genes in translocation carrier subjects III:3 and III:5

#	Gene symbol	Assay	III:3 t(3;14)		III:5 PGK1+t(3;14)		Descriptive statistics			
			NEL	Log2 FC	NEL	Log2 FC	Average	Min	Max	SD
1	*NDUFS1*	CI core sub.	9.91	-0.027	9.9	-0.003	9.97	9.62	10.43	0.263
2	*NDUFS2*	CI core sub.	10.43	0.076	10.47	0.116	10.35	10.09	10.56	0.165
3	*NDUFS3*	CI core sub.	10.06	-0.242	10.29	-0.027	10.33	10.01	10.62	0.209
4	*NDUFS7*	CI core sub.	8.17	-0.226	8.35	-0.087	8.41	8.17	8.72	0.186
5	*NDUFS8*	CI core sub.	8.81	0.156	8.97	0.331	8.65	8.43	8.94	0.169
6	*NDUFV1*	CI core sub.	10.41	-0.007	10.39	-0.006	10.40	10.33	10.51	0.056
7	*NDUFV2*	CI core sub.	8.54	-0.076	8.62	-0.011	8.64	7.66	9.92	0.681
8	*NDUFA1*	CI sup. sub.	10.20	-0.133	10.32	-0.018	10.33	9.97	10.56	0.202
9	*NDUFA2*	CI sup. sub.	10.37	-0.048	10.42	-0.001	10.44	10.06	10.66	0.170
10	*NDUFA3*	CI sup. sub.	10.5	-0.036	10.38	-0.044	10.51	10.03	10.76	0.260
11	*NDUFA4*	CI sup. sub.	8.26	-0.107	8.49	0.128	8.44	7.82	8.7	0.313
12	*NDUFA5*	CI sup. sub.	8.57	0.026	8.46	-0.021	8.62	7.9	9.25	0.386
13	*NDUFA6*	CI sup. sub.	10.22	-0.105	10.38	0.005	10.42	9.98	10.83	0.266
14	*NDUFA7*	CI sup. sub.	10.22	-0.225	10.58	0.166	10.37	10.12	10.66	0.179
15	*NDUFA8*	CI sup. sub.	9.34	-0.101	9.59	0.151	8.98	8.98	9.67	0.235
16	*NDUFA9*	CI sup. sub.	10.33	-0.031	10.39	-0.006	10.26	9.97	10.68	0.215
17	*NDUFA10*	CI sup. sub.	9.96	[a]-0.447	10.42	0.030	10.38	10.15	10.67	0.174
18	*NDUFA11*	CI sup. sub.	7.96	-0.287	8.34	0.110	8.24	7.89	8.74	0.295
19	*NDUFA12*	CI sup. sub.	10.87	0.088	10.81	0.032	10.83	10.54	11.03	0.157
20	*NDUFA13*	CI sup. sub.	8.27	-0.022	8.5	0.221	8.28	8.15	8.59	0.139
21	*NDUFAB1*	CI sup. sub.	9.11	-0.095	9.2	0.032	9.21	8.7	9.66	0.327
22	*NDUFB1*	CI sup. sub.	7.66	-0.113	7.73	-0.005	7.71	7.35	8.04	0.233
23	*NDUFB2*	CI sup. sub.	9.22	0.013	9.34	0.091	9.19	8.85	9.53	0.216
24	*NDUFB3*	CI sup. sub.	5.63	-0.306	5.86	0.033	5.82	5.2	6.27	0.338
25	*NDUFB4*	CI sup. sub.	10.44	-0.246	10.56	-0.113	10.68	10.16	10.99	0.272
26	*NDUFB5*	CI sup. sub.	11.07	-0.131	11.3	0.063	11.23	10.87	11.58	0.251
27	*NDUFB6*	CI sup. sub.	7.98	0.036	8.06	0.106	7.93	7.22	8.56	0.425
28	*NDUFB7*	CI sup. sub.	8.31	-0.140	8.49	0.061	8.44	8.23	8.8	0.177
29	*NDUFB8*	CI sup. sub.	11.44	-0.087	11.5	-0.053	11.56	11.37	11.77	0.148
30	*NDUFB9*	CI sup. sub.	9.53	-0.236	9.72	0.088	9.74	9.47	10.07	0.189
31	*NDUFB10*	CI sup. sub.	9.1	-0.178	9.48	0.185	9.29	9.03	9.71	0.240
32	*NDUFB11*	CI sup. sub.	10.53	-0.231	10.53	-0.240	10.80	10.57	11.21	0.229
33	*NDUFC1*	CI sup. sub.	9.19	0.033	9.11	0.057	9.11	8.61	9.55	0.296
34	*NDUFC2*	CI sup. sub.	10.73	-0.076	10.69	-0.106	10.80	10.18	11.11	0.302
35	*NDUFS4*	CI sup. sub.	8.67	-0.016	8.55	-0.027	8.67	8.18	9.03	0.277
36	*NDUFS5*	CI sup. sub.	11.9	-0.103	12.16	0.156	12.0	11.73	12.25	0.166
37	*NDUFS6*	CI sup. sub.	8.57	-0.174	8.96	0.248	8.71	8.25	9.13	0.302
38	*NDUFV3*	CI sup. sub.	9.1	0.030	9.05	0.016	9.03	8.9	9.26	0.106
39	*NDUFAF1*	CI ass. fact.	7.63	0.195	7.14	-0.156	7.32	6.57	7.88	0.493
40	*NDUFAF2*	CI ass. fact.	6.64	[a]-0.457	7.09	-0.138	7.12	6.84	7.36	0.144
41	*NDUFAF3*	CI ass. fact.	9.98	0.303	10.08	0.121	9.84	9.53	10.04	0.164
42	*NDUFAF4*	CI ass. fact.	9.34	0.168	9.28	0.068	9.20	8.75	9.66	0.376
43	*NDUFAF5* *C20ORF7*	CI ass. fact.	7.23	0.030	6.75	-0.001	7.01	6.64	7.37	0.275
44	*NDUFAF6* C8ORF38	CI ass. fact.	5.44	-0.174	5.84	0.046	5.63	5.07	6.36	0.377
45	*AIFM1*	CI ass. fact.	9.15	-0.178	9.38	0.068	9.41	8.97	9.77	0.243
46	*ECSIT*	CI ass. fact.	8.22	-0.22	8.23	-0.092	8.39	8.26	8.6	0.126
47	*F0XRED1*	CI ass. fact.	9.07	0.093	8.74	-0.082	8.75	8.43	9.48	0.374
48	*PHB*	CI ass. fact.	10.42	-0.216	10.33	-0.278	10.56	9.89	11.06	0.325
49	*PTCD1*	CI ass. fact.	7.83	-0.008	7.67	-0.153	7.82	7.72	8.03	0.096
50	***NUBPL***	CI ass. fact.	7.81	-0.160	7.6	-0.292	7.92	7.62	8.31	0.213

Include 7 CI core subunits (#1-7), 31 CI supernumerary subunits (#8-38), and 12 CI assembly factors (#39-46) (according to [Fassone and Rahman 2012; Calvo et al, 2010). NEL normalized expression level. Translocation carriers were compared individually to a control group. [a]Difference greater than 2 SD.

Table S7. Main interactions of the amino acid involved in the mutation.

Residue	Open conformation[a]			Closed conformation[b]		
	Hydrogen/ionic interactions	Hydrophobic interactions	Solvent accessible[c]	Hydrogen/ionic interactions	Hydrophobic interactions	Solvent accessible[c]
E120			yes	OE1 →S77 OG OE2 →L78 N		yes

Residue E120 is solvent accessible and in the closed conformation of the protein makes hydrogen bonds with Ser77 and Leu78 of the loop connecting β-strand B with the helix 2 (Fig. S5). [a]Atomic coordinates of Protein Data Bank entry 2XE7; [b]atomic coordinates of Protein Data Bank entry 2WZC; [c]calculated with the CCP4 Suite, residues are considered solvent accessible when accessible surface area is > 5 Å.

Supplementary references

Antony D, Becker-Heck A, Zariwala MA, et al, 2013 Mutations in *CCDC39* and *CCDC40* are the major cause of primary ciliary dyskinesia with axonemal disorganization and absent inner dynein arms. *Hum Mutat* 34:462-72.

Balog E, Laberge M, Fidy J 2007 The influence of interdomain interactions on the intradomain motions in yeast phosphoglycerate kinase: a molecular dynamics study. *Biophys J* 92:1709-16.

Kevelam SH, Rodenburg RJ, Wolf NI, et al, 2013 NUBPL mutations in patients with complex I deficiency and a distinct MRI pattern. *Neurology* 80:1577-83.

Kiedrowski LA, Raca G, Laffin JJ, Nisler BS, Leonhard K, McIntire E, Mongomery KD 2011 DNA methylation assay for X-chromosome inactivation in female human iPS cells. *Stem Cell Rev* 7:969-75.

Li H and Durbin R 2009 Fast and accurate short read alignment with Burrows-Wheeler transform. *Bioinformatics* 25:1754-60.

Li H, Handsaker B, Wysoker A, et al 1000 Genome Project Data Processing Subgroup 2009 The sequence alignment/map format and SAMtools. *Bioinformatics* 25:2078-9.

Merveille AC, Davis EE, Becker-Heck A, et al, 2011 CCDC39 is required for assembly of inner dynein arms and the dynein regulatory complex and for normal ciliary motility in humans and dogs. *Nat Genet* 43:72-78.

Ordulu Z, Wong KE, Currall BB, et al 2014 Describing sequencing results of structural chromosome rearrangements with a suggested Next-Generation Cytogenetic nomenclature. *Am J Hum Genet* 94:695-709.

Vas M, Varga A, Gráczer E 2010 Insight into the mechanism of domain movements and their role in enzyme function: example of 3-phosphoglycerate kinase. *Curr Protein Pept Sci* 11:118-47.

Wortmann SB, Kluijtmans LA, Engelke UFH, et al 2012 The 3-methylglutaconic acidurias: what's new? *J Inherit Metab Dis* 35:13-22.

Szilágyi AN, Vas M 1998 Anion activation of 3-phosphoglycerate kinase requires domain closure. *Biochemistry* 37:8551–63.